Adv Polym Sci (2009) 222: 115–173
DOI:10.1007/12_2008_2

Published online: 4 March 2009

Molecular Processing of Polymers with Cyclodextrins

Alan E. Tonelli

Abstract We summarize our recent studies employing the cyclic starch derivatives called cyclodextrins (CDs) to both nanostructure and functionalize polymers. Two important structural characteristics of CDs are taken advantage of to achieve these goals. First the ability of CDs to form noncovalent inclusion complexes (ICs) with a variety of guest molecules, including many polymers, by threading and inclusion into their relatively hydrophobic interior cavities, which are roughly cylindrical with diameters of $\sim 0.5 - 1.0$ nm. α-, β-, and γ-CD contain six, seven, and eight α-1,4-linked glucose units, respectively. Warm water washing of polymer-CD–ICs containing polymer guests insoluble in water or treatment with amylase enzymes serves to remove the host CDs and results in the coalescence of the guest polymers into solid samples. When guest polymers are coalesced from the CD–ICs by removing their host CDs, they are observed to solidify with structures, morphologies, and even conformations that are distinct from bulk samples made from their solutions and melts. Molecularly mixed, intimate blends of two or more polymers that are normally immiscible can be obtained from their common CD–ICs, and the phase segregation of incompatible blocks can be controlled (suppressed or increased) in CD–IC coalesced block copolymers. In addition, additives may be more effectively delivered to polymers in the form of their crystalline CD–ICs or soluble CD–rotaxanes. Secondly, the many hydroxyl groups attached to the exterior rims of CDs, in addition to conferring water solubility, provide an opportunity to covalently bond them to polymers either during their syntheses or via postpolymerization reactions. Polymers containing CDs in their backbones or attached to their side chains are observed to more readily accept and retain additives, such as dyes and fragrances. Processing with CDs can serve to both nanostructure and functionalize polymers, leading to greater understanding of their behaviors and to new properties and applications.

A.E. Tonelli (✉)
Fiber & Polymer Science Program, North Carolina State University, Campus Box 8301, Raleigh, NC 27695-8302, USA
e-mail: alan_tonelli@ncsu.edu

Keywords Additives, Blends, Complexation processing, Cyclodextrins, Polymers, Threading

Contents

1 Introduction

Though cyclodextrins (CDs) had long been known to form both soluble and crystalline inclusion compounds (ICs) with a variety of small molecule guests, Harada and Kamachi first demonstrated in 1990 [1], using poly(ethylene oxide) (PEO) oligomers, that noncovalent bonded crystalline ICs could be formed between guest polymers and host CDs as well. This is accomplished by threading of the guest polymers through the CD cavities to form polymer threaded crystalline stacks, as illustrated in Fig. 1f. CDs are cyclic molecules formed by six (α-CD), seven (β-CD), and eight (γ-CD) α-1,4-linked glucose units, with internal hydrophobic cavities of $\sim 0.5 - 1.0$ nm in diameter (Fig. 1a). Their 18–24 hydroxyl groups are located on the CD rims making them soluble in water.

Since the middle of the 1990s our research group has formed a large number of crystalline CD–ICs [2–70] containing either high molecular weight guest polymers or small-molecule guests that can serve as polymer additives (Fig. 1c–f). The motivation for our studies is threefold. First, polymer chains included in CD–ICs are necessarily both highly extended and isolated from neighboring chains, because they are threaded through and confined in the narrow CD channel cavities (see Fig. 1a, f). As suggested in Fig. 2, if the host CDs in polymer-CD–ICs are carefully removed and the guest polymer chains are permitted to coalesce into a bulk solid sample, then

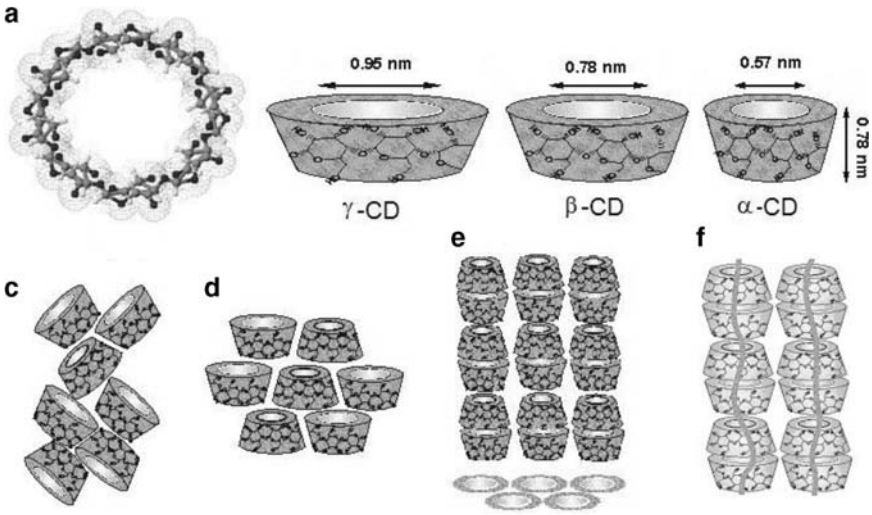

Fig. 1 (**a**) γ-CD chemical structure and approximate dimensions of α-, β-, and γ- CDs; schematic representation of packing structures of (**c**) cage-type, (**d**) layer-type, and (**e**) head-to-tail channel-type CD crystals; and (**f**) CD–IC channels containing included polymer guests

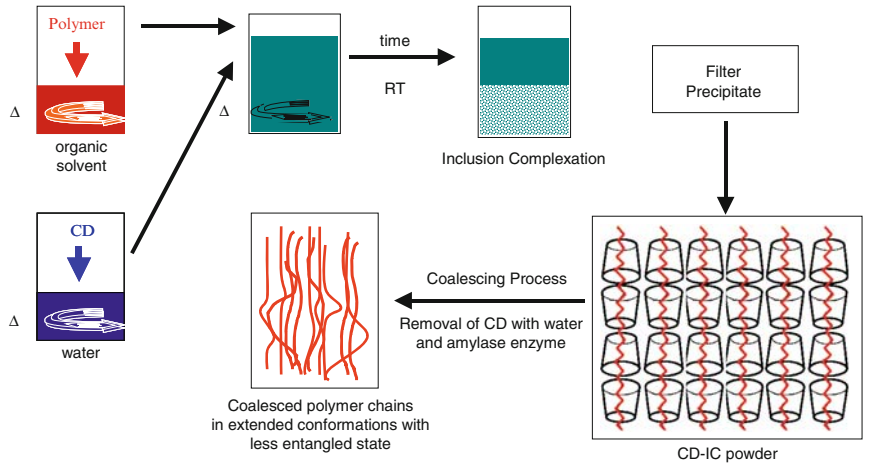

Fig. 2 Schematic representation of polymer-CD IC formation, the coalescence process, and the coalesced polymer

it can be reasonably expected that the arrangement of chains, or their packing, might be significantly different from those normally produced from their randomly coiling and entangled solutions or melts. This expectation has been confirmed numerous times in our laboratory.

Processing with CDs can serve to both nanostructure and functionalize polymers, leading to greater understanding of their behaviors and to new properties and

applications. In fact, we generally observe upon coalescence from their CD–ICs that (1) crystallizable homopolymers evidence increased levels of crystallinity, unusual polymorphs, and higher melting, crystallization, and decomposition temperatures, while amorphous homopolymers exhibit higher glass-transition temperatures, than samples consolidated from their disordered solutions and melts; (2) molecularly mixed, intimate blends of two or more polymers that are normally believed to be immiscible can be obtained from their common CD–ICs, (3) the phase segregation of incompatible blocks can be controlled (suppressed or increased) in coalesced block copolymers, and (4) the thermal and temporal stabilities of the coalesced and well-mixed homopolymer blends and block copolymers appear to be substantial, thereby suggesting retention of their as-coalesced structures and morphologies under normal thermal processing conditions.

Because crystalline CD–ICs are high-melting and thermally stable, even when containing small-molecule guests that are volatile liquids or even gases in the bulk, delivery of additives to polymer materials can be improved by using additive-CD–ICs, which may often be conveniently melt-processed into polymers. If we begin with appropriate soluble CD–ICs formed with polymer additives and then react the free ends of the included additive with capping groups that prevent it from unthreading, we create CD–rotaxanated additives. One advantage of additive-CD–rotaxanes is the protection (thermal, chemical, UV–Vis, etc.) afforded by their CD coats. Another is the ability to utilize the many hydroxyl groups on the CD coat to target the delivery of the CD-additive–rotaxane to a particular polymer substrate.

Our second motivation for utilizing CDs with polymers is to alter their functionalities through incorporation of CDs into their backbones during polymerization or to attach them to polymer side chains via postpolymerization reactions. The presence of covalently bonded CDs in polymers serves to increase their acceptance and retention of additives, such as dyes, fragrances, antibacterials, etc. They may also be further reacted or treated through their covalently bonded CDs to cross-link and form networks or to form blends with other polymers having a propensity to thread through their attached CD cavities.

Thirdly, CDs are nontoxic, biodegradable, and bioabsorbable, and, as such, may be used in medical applications and as materials more friendly to the environment.

As indicated above, in this report we summarize our recent studies employing cyclodextrins (CDs) to both nanostructure and functionalize polymer materials.

2 Experimental

2.1 Polymer-CD–ICs

CD–ICs formed with polymer guests are crystalline solids (see Fig. 1f), which may be formed by mixing host CD solutions (usually aqueous) with guest polymer solutions (usually nonaqueous and organic) with the aid of heating, stirring, and

sonication [6]. Solid CDs may also be suspended in polymer solutions [24, 41, 71] or neat bulk liquid polymers [45, 72] to form polymer-CD–ICs. Because native CDs with only water of hydration included in their cavities assume herringbone or brick-type crystal structures illustrated in Fig. 1c, d, while polymer-CD–ICs assume the very different columnar, channel structure shown in Fig. 1e, f, X-ray diffraction is utilized to test for successful polymer-CD–IC formation. This is supplemented by DSC, FTIR, and solid-state ^{13}C-NMR observations to confirm that polymer is present and included in the CD–ICs formed.

Warm water washing of polymer-CD–ICs containing polymer guests insoluble in water or treatment with amylase enzymes serves to remove the host CDs and results in the coalescence of the guest polymers into solid samples. X-ray diffraction, DSC, TGA, and FTIR and NMR spectroscopies are typically used to characterize the coalesced polymer samples.

2.2 Additive-CD–ICs and –Rotaxanes

Crystalline CD–ICs with low molecular weight additive guests, both soluble and crystalline, may be prepared [7, 9, 13, 17, 52, 53, 65, 68–70] by virtually the same means as polymer-CD–ICs. Corresponding soluble CD–rotaxanes can be obtained from soluble CD–ICs, by attaching bulky end-groups to both ends of the included additive or by extending the CD cavity, thereby preventing the unthreading of the additive. An example of the synthetic route for obtaining an azo-dye-α-CD–rotaxane will be subsequently discussed.

3 Nanostructuring/Functionalizing Polymers via CD–IC Formation and Coalescence and Additive Delivery with Additive-CD–ICs and –Rotaxanes

3.1 Nanothreading of Polymers [55, 73, 74]

Before presenting and discussing our results concerning the processing of polymers with CDs, it seems appropriate to discuss several experiments designed to determine those factors important to the nanothreading of polymers with CDs during the process of forming polymer-CD–ICs, and which were recently summarized [55, 73, 74]. These include (1) the competitive CD threading of polymers with different chemical structures and molecular weights from their solutions containing suspended solid or dissolved CDs, (2) the threading and insertion of undiluted liquid polymers into solid CDs, and (3) suspension of IC crystals containing polymer A or B in a solution of polymer B or A and observation of the exchange of polymers between the solution

and the CD–IC crystals, without dissolution of the CD–ICs. The reader is also referred to the recent work of Gerhard Wenz [75].

3.1.1 Competitive Threading

Two studies were conducted to probe the potential for using the complexation of polymers with CDs as a means to separate them according to their molecular weight (MW) or chain lengths [11, 15]. In the first investigation two poly(ethylene glycol) (PEG) samples, with MW = 600 (PEG600) and 20,000 (PEG20000) and narrow MW distributions of 1.1 and 1.34, respectively, were dissolved in water and added to an aqueous solution of α-CD to form PEG-α-CD–ICs. α-CD–ICs were separately formed with PEG600, PEG20000, and with various mixtures of the two PEG samples. By comparing the viscosities of their solutions after filtering off the PEG-α-CD–ICs formed, it was found that the PEG-α-CD–IC formed from an equimolar PEG600/PEG20000 solution, using enough α-CD to complex either all of one or half of each PEG, contained 80% of the higher molecular weight PEG20000.

The second study compared the α-CD–ICs formed in solution with poly(ε-caprolactone) (PCL) and hexanoic acid (HA), which closely mimics the PCL repeat unit [15]. FT–IR observations of the α-CD–ICs formed with PCL, HA, and PCL/HA mixtures were used to determine the presence of PCL and HA guests (PCL and HA C = O stretching bands at 1,734 and 1,714 cm^{-1}, respectively). Both guests were observed to be equally present in the α-CD–ICs when equal amounts of PCL and HA were mixed with enough α-CD to complex both guests. However, when half the amount of α-CD was used, i.e., enough to complex all of the PCL, or all of the HA, or half of each, PCL was observed to be predominantly included.

Thus, both studies showed a preference for the inclusion of the longer, higher MW guest polymer, irrespective of their very different chemical natures: PEGs are hydrophilic and soluble in water, while PCL and HA are not. This suggests that the formation of α-CD–ICs in solution with both PEG and PCL guests may be dominated by the kinetics of the process, which favors higher MW, longer guests. It was suggested that longer polymer chains partially threaded with CDs would nucleate the growth of polymer-CD–IC crystals more readily than partially threaded shorter chains, because the unthreading of CDs from the longer chains would be slower or retarded compared with the unthreading of CDs from the shorter chains.

The dependence of CD–IC formation from solution for polymers with different stereosequences was investigated for isotactic (i) and atactic (a) poly(3-hydroxybutyrates) (i-PHB and a-PHB) [26]. i-PHB was found to form an IC with α-CD, but not with β- or γ-CDs, while only γ-CD formed an IC with a-PHB. From these observations it was concluded that extended conformations available to i-PHB were too narrow, thin for a tight-packing fit with β- or γ-CDs, while the much wider, thicker extended conformations available to a-PHB chains precluded their inclusion in the narrower α- and β-CDs, but fit tightly in the more spacious channels of its IC formed with γ-CD.

The solution complexation of PCL and the related aliphatic polyester poly(L-lactic acid) (PLLA) with CDs was studied [29]. PCL was observed to be able to form ICs with both α- and γ-CDs, with the latter containing two PCL chains in each γ-CD channel, while only α-CD formed an IC with PLLA. When a solution containing equivalent amounts of PCL and PLLA was added to an aqueous solution containing enough α-CD to complex with all of the PCL, or all of the PLLA, or half of each, only PCL-α-CD–IC was formed. Furthermore, when a PCL solution was added to an aqueous solution containing the same molar quantities of α- and γ-CDs, each sufficient to fully complex with the added PCL, only PCL-α-CD–IC was formed. These observations led to the following tentative conclusions: (1) interactions between extended and included PCL chains and α-CD may be more favorable than the average of the interactions between the two parallel side-by-side PCL chains included in PCL-γ-CD–IC and the two included PCL chains with γ-CD, or the double-threading of PCL chains required to form the PCL-γ-CD–IC might retard the kinetics of its formation, (2) interactions between included PCL chains and α-CD channels are more favorable than those involving PLLA, (3) differences in PCL/solvent and PLLA/solvent interactions are not important, and (4) the preference of PCL over PLLA inclusion by α-CD is not a consequence of a difference in the cross-sections of their extended conformations nor a difference in the kinetics of their threading by α-CD, because the PLLA sample consisted of longer chains than the PCL sample.

3.1.2 Threading of Polymers into Solid CDs

We have discovered a simple precipitation method for forming solid CDs in an empty channel structure, CD_{CS} (see Fig. 1e), containing no complexed guest aside from water of hydration [24, 71]. When propionic acid (PA), which in solution forms a cage structure α-CD–IC (see Fig. 1c) with dissolved α-CD, is dissolved in a nonsolvent for α-CD and α-CD_{CS} is suspended therein, PA entered α-CD_{CS} and transformed it to a cage structure PA-α-CD–IC. However, when α-CD_{CS} was vacuum-dried before suspension in the same PA solution, a columnar structure PA-α-CD–IC was formed. Clearly the role of water, some of which is displaced from the air-dried α-CD_{CS} channels upon inclusion of PA, is important in the formation of CD–ICs, as well as the packing interactions between host α-CDs. Apparently the vacuum drying of a-CD_{CS} stabilizes the packing of α-CDs in the columnar structure, because as PA is included, the solid state transformation to a cage structure PA-α-CD–IC is prevented. α- and γ-CD–ICs formed with PCL were suspended in acetone and aqueous solutions of γ- and α-CDs, respectively [29]. In the first case nothing happened, but in the second case the PCL chains in suspended PCL-γ-CD–IC dissociated, unthreaded, and were instead complexed with α-CD to form PCL-α-CD–IC.

In another set of experiments [29], PCL- and PLLA-α-CD–ICs were suspended in dioxane solutions initially containing dissolved PLLA and PCL, respectively. After several days the suspended α-CD–ICs crystals were filtered out and observed by FT–IR (distinct C = O absorption bands of PCL and PLLA) to determine whether

PCL, PLLA, or both were included. The α-CD–IC resulting from the suspension of PLLA-α-CD–IC in the PCL solution was found to contain only PCL guest chains, while the α-CD–IC resulting from the suspension of PCL-α-CD–IC in the PLLA solution contained only a very small amount of PLLA guest chains. The above results were interpreted to signify the importance of both guest polymer hydrophobicity and guest/host steric compatibility in the formation of polymer-CD–ICs.

The ability of poly(N-acylethylenimine) (PNAI) to be complexed from its solutions containing suspended cage and columnar structure γ-CDs was investigated [41]. PNAIs with two different MWs were synthesized and two different PNAI solvents (acetone and chloroform) were employed. Complexation of the PNAIs from solutions containing suspended γ-CDs was directly monitored by ^{1}H NMR, as shown in Fig. 3. The time-dependent intensities of PNAI and water ^{1}H resonances were observed and permitted an evaluation of the kinetics of the PNAI inclusion.

In the acetone solutions the inclusion of PNAIs by columnar γ-CD_{CS} was greater in both quantity and speed than for cage γ-CD (Fig. 4). In both cases PNAI inclusion was accomplished without any dissolution of the suspended γ-CDs, because

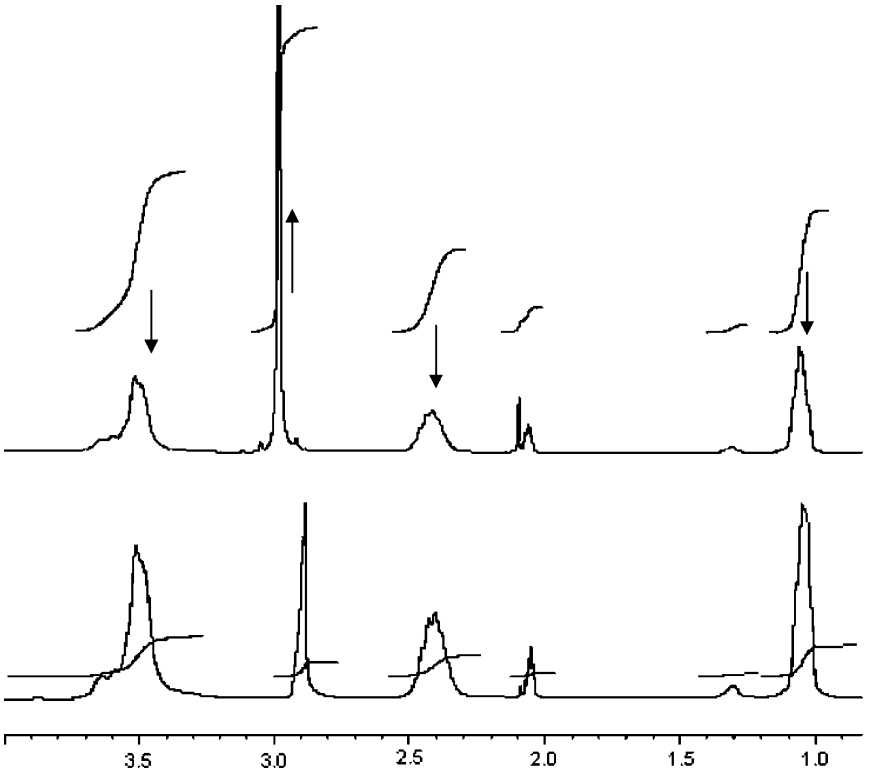

Fig. 3 Time-dependent ^{1}H-NMR spectra of PNAI-1 in acetone solution containing settled, initially cage structure γ-CD: *bottom* (initial); *top* (after 90 h). *downward arrow*, *upward arrow* = decreasing, increasing PNAI, H_2O peak intensities

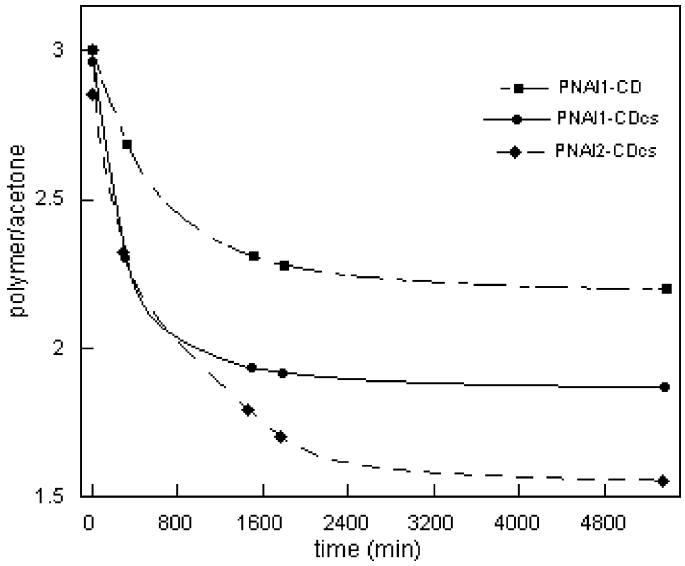

Fig. 4 Decrease of polymer peak intensities with time as a result of inclusion in cage γ-CD or in columnar $\gamma - CD_{CS}$. PNAI2 has a higher molecular weight than PNAI1

^{1}H resonances were never observed for dissolved γ-CDs. In comparison to the lower MW sample, more of the higher MW PNAI was included in γ-CD_{CS}, but the rate of PNAI inclusion was the same for both samples. Of the six water molecules residing in the channels of each γ-CD_{CS} [24,71], only two were observed to be removed upon inclusion of the PNAI guest chains. Furthermore, when the γ-CDs were suspended in chloroform solutions of the PNAIs, no ejection of hydration water nor inclusion of PNAI chains was observed.

Thus, the inclusion of PNAIs in suspended γ-CDs was both thermodynamically and kinetically preferred in the case of γ-CD_{CS}, while the inclusion of high MW PNAI is apparently thermodynamically favored. Using chloroform as a solvent for PNAI and as a suspension medium for the γ-CDs prevented PNAI inclusion, presumably because of the unfavorable environment provided by chloroform for the potentially displaced and ejected water. By comparison to the estimated increase in conformational free energy experienced by randomly coiling polymers as they are extended and confined in γ-CD channels [76], which is mainly entropic in origin, it could be estimated that each water molecule ejected during PNAI inclusion in γ-CD_{CS} must lower its free energy by at least $\sim 1\,\mathrm{kcal\,mol^{-1}}$ to offset the loss of conformational entropy of the included polymer.

PEG oligomers (MWs = 200 and 400), which are liquids at room temperature, were mixed with solid, native cage structure α-CD and observed by X-ray diffraction to convert to columnar structure PEG-α-CD_{CS} [45,72]. An example is presented in Fig. 5, where the scattering peaks at $2\theta \sim 12$ and $\sim 20^\circ$, characteristic [6] of cage α-CD and columnar α-CD_{CS}, respectively, are observed to decrease and increase

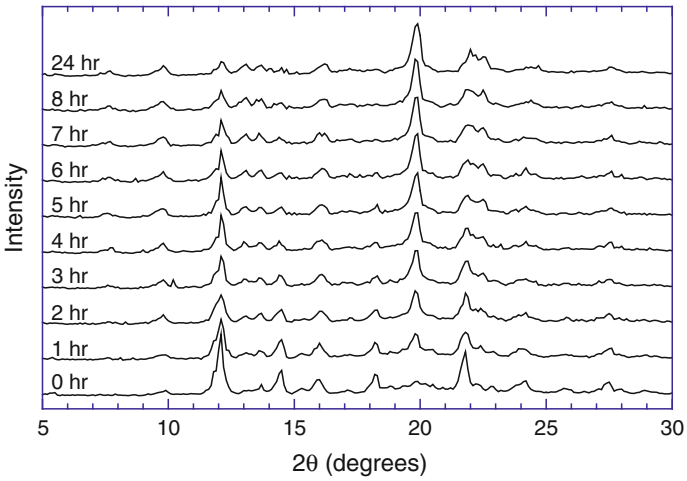

Fig. 5 Time-dependent diffractometer scans for a 2:1 mixture of PEG200:α-CD obtained at 20°C [45, 72]

over time as the liquid PEG threads into the solid α-CD crystals. Both the time and temperature dependences of the solid-state conversion of cage to columnar structure α-CD through inclusion of bulk liquid PEG oligomers were investigated. An activation energy of 8.3 kcal mol^{-1} of α-CD was determined from the observed temperature dependence of inclusion kinetics. Increasing the PEG/α-CD ratio increased the rate of PEG inclusion, while increasing the MW of PEG slowed the inclusion. Drying the as-received cage structure α-CD before mixing with the PEG oligomers had little effect on the rate of PEG inclusion. More recent observations indicate that the rate and extent of PEG inclusion may be affected by the degree of α-CD hydration [77].

In addition, native cage α-CD was suspended in acetone solutions of the PEGs, and its solid-state conversion to channel structure as PEG chains were included and formed PEG-α-CD–IC crystals was observed by solution ^{1}H NMR. The rate of PEG inclusion from solution was ∼10-times faster than the rate observed for the neat PEGs, even though the PEG concentration in solution was only ∼1% that of neat PEG.

These observations may be generally summarized as follows: as the mobility of PEG increases, i.e., moving from neat to dissolved PEG and/or from higher to lower MW, so does the rate of inclusion of PEG into suspended cage α-CD via the solid–solid cage-to-columnar crystal structure transition. Since drying the as-received cage structure α-CD did not affect the rate of its transition to columnar α-CD, α-CD_{CS}, by the inclusion of neat PEG, apparently this process is not sensitive to the internal hydration level of the suspended cage structure α-CD. However, the water vapor content in the atmosphere surrounding the solid α-CD and liquid PEG was recently shown [77] to have a significant effect.

The inclusion of neat and dissolved PEG oligomers into suspended columnar α-CD_{CS}, was preliminarily observed by DSC and solution ^{1}H NMR [45, 72] to proceed at much faster rates than inclusion by suspended cage structure α-CD, because of the absence of the need to transform the solid-state packing of α-CDs upon inclusion of PEG. As a consequence, analysis of the temperature-dependent kinetics of PEG oligomer inclusion in α-CD_{CS} enabled [76] an experimental assessment of the free energy change experienced by randomly coiling PEG oligomers as they are extended and thread into the narrow α-CD_{CS} channels.

Extension of the investigations summarized here should eventually permit a more complete answer to the question "Why do randomly coiling polymer chains in solution or the neat melt become threaded or thread into the nano-pores of dissolved or solid CDs, where they are highly extended and segregated from other polymer chains?" However, we can currently conclude that electrostatic, van der Waals, and hydrogen-bonding interactions and relief of conformational strain in CDs are not important, while hydrophobic interactions, exclusion of high energy, cavity-bound water, and crystalline packing of host CDs are important in the formation of polymer-CD–ICs.

4 Polymers Coalesced from their CD–ICs

4.1 Homopolymers Coalesced from their CD–ICs

4.1.1 Poly(ethylene terephthalate) [21, 33, 59]

When PET chains are included in the ∼1.0 nm channels of its γ-CD–IC [21] they adopt kink conformations, as drawn in Fig. 6, which are nearly as extended, but are narrower in cross-section than the crystalline all trans PET conformation also shown. Upon coalescence from its γ-CD–IC, PET rapidly crystallizes, achieving

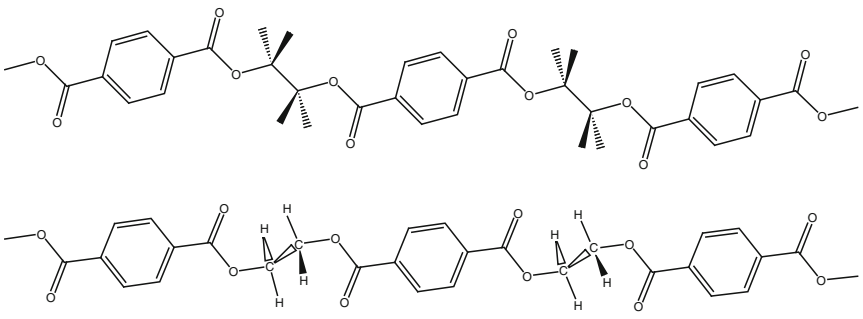

Fig. 6 All trans (*top*) and g±tg∓ kink (*bottom*) conformations of crystalline and IC-included PET chains, respectively

Table 1 PET Film Densities [59]

Sample	Density (ρ)[g cm^{-3}]	Crystallinity from DSC	Crystallinity from X-ray
Coalesced PET	1.3670	0.39	0.32
Annealed as-received PET	1.3497	0.39	0.31
As-received PET	1.3497	0.10	0.06

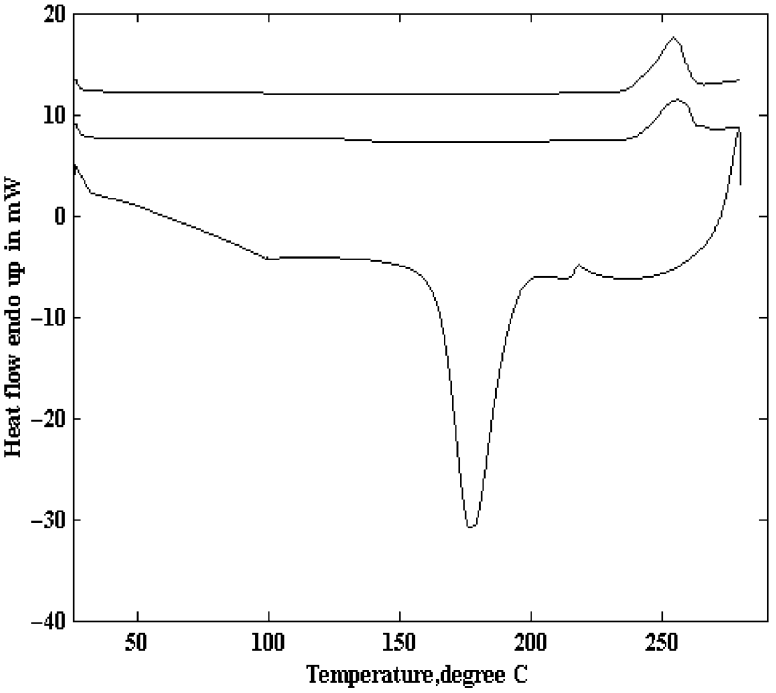

Fig. 7 DSC thermogram of coalesced PET. First (*upper*), second (*middle*) heating and (*lower*) interim cooling scans. (Note that the heat flow units on the ordinate are only appropriate for the cooling scan and that the magnitudes of the melting endotherms and crystallization exotherm obtained from them are actually nearly identical.) PETs normally processed from their solutions and melts, on the other hand, do not evidence recrystallization upon rapid cooling (-200°C min^{-1}) from their melts [33]

$\sim$40% crystallinity (see Table 1, for typical levels of crystallinity in PET), while solid-state FTIR and NMR observations presented later [21, 33] indicate that the PET chains in the noncrystalline regions of coalesced PET largely retain their included kink conformations.

The reorganized morphology of the coalesced PET is manifested in its thermal behavior, as presented in the DSC scans shown in Fig. 7. Note that no glass-transition or crystallization is observed in either heating scan, with the former observation receiving support from temperature-dependent solid-state NMR relaxation

observations discussed below [33]. Instead, both heating scans simply evidence a large melting endotherm, indicating substantial crystallinity for the coalesced PET both after coalescence and subsequent to rapid cooling from the melt. In summary, including PET chains in and coalescing them from its γ-CD–IC has reorganized them into a sample that is repeatedly and rapidly crystallizable from its melt, with noncrystalline regions that do not show a T_g, behavior that is normally very uncharacteristic of usually amorphous and slow to crystallize PET.

This contrasting thermal behavior for coalesced and normal PETs is further emphasized in the density results presented in Table 1. There the densities measured for as-received PET before and after high temperature annealing (110°C for 30 min) are compared with the density of the coalesced sample. Not surprisingly the densities of both the annealed and coalesced samples are higher than that of the as-received PET, because the former samples are more crystalline than the latter one. What is initially surprising, however, is even though the annealed and coalesced PET samples have closely similar levels of crystallinity, the density of the coalesced sample is much higher. Thus, it appears that the PET chains in the noncrystalline regions of the coalesced PET film are more densely packed (by ∼1.4%) than in the amorphous regions of the annealed PET film, even though each film is ∼65% noncrystalline. The coalesced PET film has a higher density noncrystalline phase, because there the chains are more extended and tightly packed, and possibly more oriented, with a higher trans conformer content for the -CH_2–CH_2- bonds (FTIR results presented below [21]). In fact, the density estimated for the noncrystalline regions in coalesced PET ($\rho_{nc} = 1.354\,g\,cm^{-3}$) exceeds slightly the overall density of the annealed PET film ($1.3497\,g\,cm^{-3}$).

In Fig. 6 both the all trans crystalline conformation of PET and noncrystalline, though also highly extended, kink conformation of PET are drawn. PET chains in the narrow channels of its γ-CD–IC crystals adopt the kink conformations, which after coalescence were also demonstrated to persist in the noncrystalline regions [21, 33, 59]. PET kink conformers have been suggested to occupy only ∼2/3 of the volume occupied by the all trans crystalline PET conformation [78]. If the kink conformers also dominate the noncrystalline regions of coalesced PET, then the observation that $\rho_{nc} = 1.354\,g\,cm^{-3}$ exceeds the overall density of annealed PET, $\rho_{anneal} = 1.3497\,g\,cm^{-3}$, may be understood. In addition, the kink conformations adopted by PET included in its γ-CD–IC may upon coalescence be easily and rapidly converted into the crystalline all trans conformation solely by facile counter rotations about the -O–CH_2- and -CH_2–O- bonds, a conformational transformation producing little swept out volume and resulting in a highly crystalline sample. Largely amorphous as-received PET, on the other hand, is slow to crystallize, because its largely gauche -CH_2–CH_2- bonds must be rotated to the trans conformation during crystallization, a conformational transformation that must sweep out a large volume [21].

The FTIR spectra (Fig. 8) of as-received and solution-cast PET samples, although very similar, are clearly distinct from the spectrum of coalesced PET. The most noticeable difference is the much improved resolution observed in the spectrum of PET coalesced from its γ-CD–IC, in which nearly every vibrational absorption,

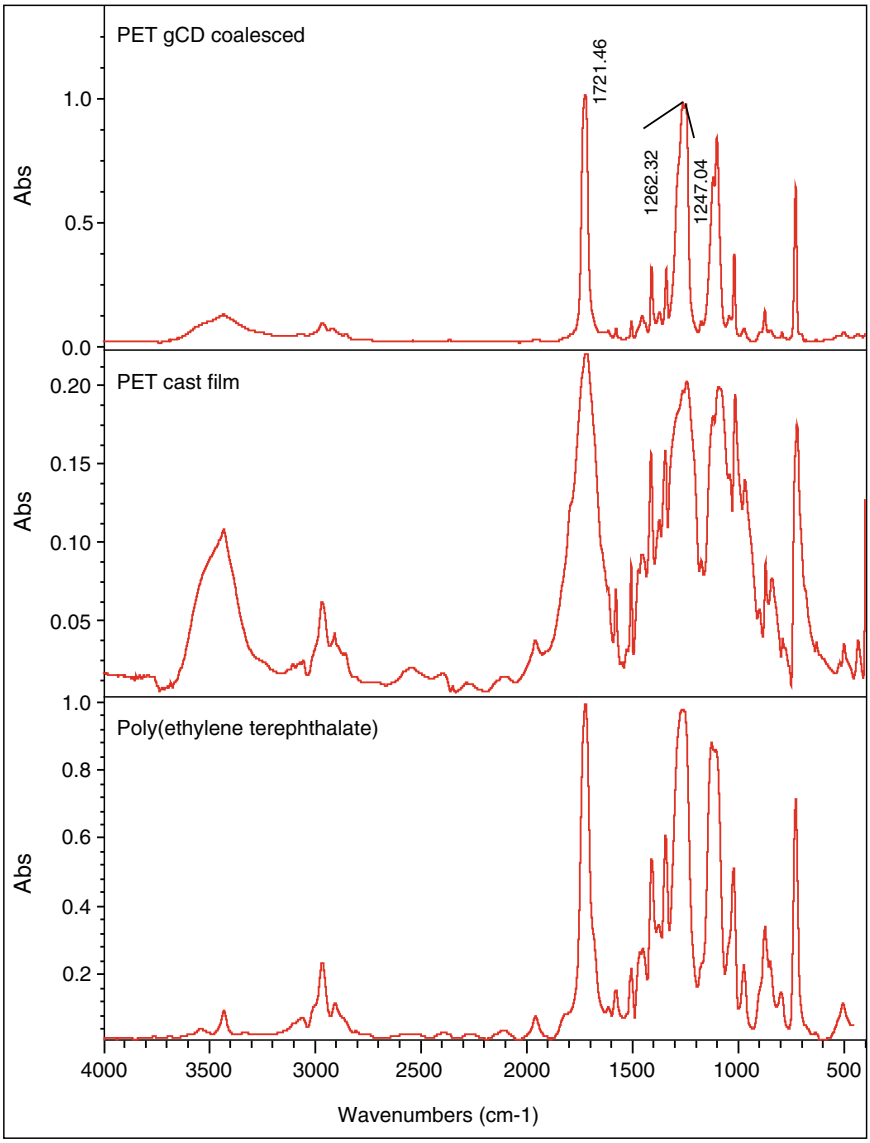

Fig. 8 FTIR spectra of as-received PET (melt-extruded pellets [21]), solution-cast PET, and IC-coalesced PET samples, from *bottom* to *top*, respectively [21]

except those likely contributed by residual γ-CD or H_2O above 3,200 cm^{-1}, is resolved to the baseline. This improved resolution may be a result of the already suggested improved order in the noncrystalline regions of the sample; the chains are not as nearly randomly coiling or interpenetrating as those in the noncrystalline regions of the as-received and solution-cast samples and, as a result, do not exhibit

a glass transition (DSC and solid-state NMR [33] below). The generally broad IR bands observed in polymer samples are undoubtedly due to the large variety of polymer conformations and chain-packing environments surrounding each vibrating molecular bond or group. Because of the improved order in the noncrystalline regions of the coalesced PET, vibrating molecular bonds and groups are subjected to smaller variations in their local conformational and packing environments.

For example, a clear doublet band can be seen at 1,247 and 1,262 cm^{-1} in the coalesced PET spectrum, possibly reflecting crystal or correlation field splitting generally produced by short-range interchain interactions [79, 80] between closely packed molecules in their crystals. Because both X-ray (not shown [21]) and DSC observations indicate very similar crystal structures for the solution-cast and coalesced PET samples, this vibrational band splitting may instead be occurring in the noncrystalline regions of the coalesced sample, as a result of distinct short-range interactions between pairs of PET chains adopting the highly extended narrow and noncrystalline kink conformations, which may permit PET chains to be in closer contact than the all-trans chains in their crystals. In fact, these vibrations have been associated [81] with the terephthaloyl residues of PET in the amorphous sample portions [82], with the 1,247 cm^{-1} vibration appearing as a shoulder on the 1,262 cm^{-1} band. Because these bands appear as a distinct doublet in the coalesced PET spectrum, a more homogeneous population of conformations is suggested for the noncrystalline chains, which are also apparently quite tightly packed with the terephthaloyl residues of neighboring chains in close proximity. The distinct morphologies of melt-crystallized as-received and coalesced PETs are made clear in Fig. 9, where their polarized micrographs are presented. Though both samples were crystallized from their melts, more uniformly distributed much smaller crystallites are evident in the coalesced PET sample. The as-received PET formed typical large spherulites after crystallization from the melt, which have spherical shapes and dark crosses through their centers when viewed with polarized light. The average size of the as-received PET spherulites is about 25 μm. In contrast, the morphology of PET coalesced from its γ-CD inclusion complex and subsequently crystallized from its melt shows a distinct crystal pattern without clear spherical shapes. Under polarized light, the coalesced, melt-crystallized PET shows much less dark areas than the as-received PET, although both samples were crystallized from their melts under the same conditions.

Because the crystallization of polymers from their melts is related to their microstructural properties, such as chain conformations and entanglements [83], the polarized light microscopy results suggests a molecular-level difference between the coalesced and as-received PETs even in their melts.

In Fig. 10 the high-resolution ^{13}C-NMR spectra observed for various solid PET samples are presented [33]. Consistent with our molecular modeling [78, 84] and FTIR [21] results, the solid-state NMR spectra indicate that as-received PET has predominantly $g\pm$ -CH_2–CH_2- bonds and substantial amounts of t -CH_2–O- and -O–CH_2- bonds, while coalesced, included, and precipitated PETs have preponderantly t -CH_2–CH_2- and $g\pm$ -CH_2–O- and -O–CH_2- bonds. (Details are presented as part of [33]).

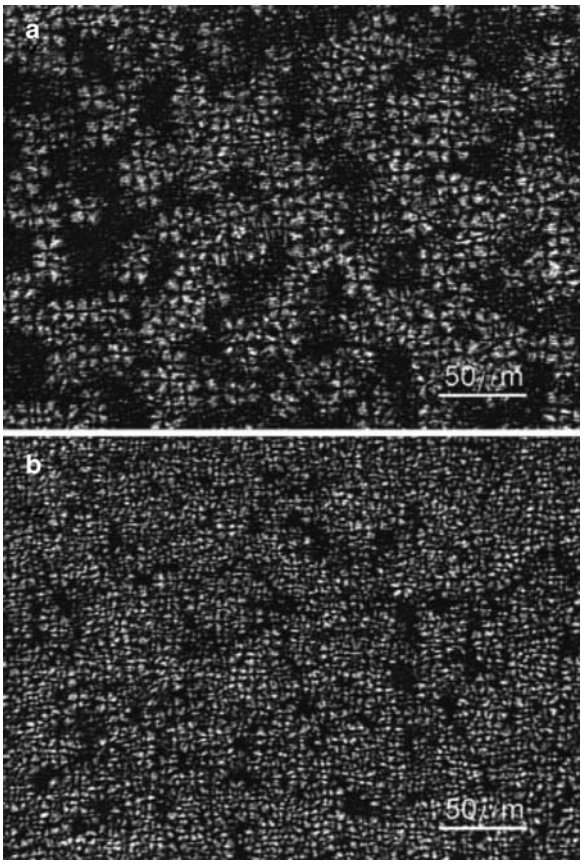

Fig. 9 Polarized light micrographs of melt-crystallized (**a**) as-received PET and (**b**) coalesced PET [33]

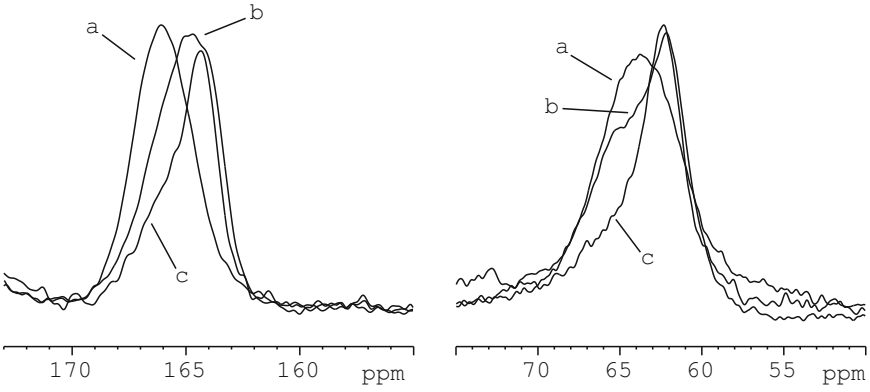

Fig. 10 Methylene carbon (∼60–65 ppm vs. TMS) and carbonyl carbon (∼163–168 ppm vs. TMS) resonance peaks for PETs: (**a**) as received PET; (**b**) precipitated PET; (**c**) coalesced PET or PET-γ-CD–IC [33]

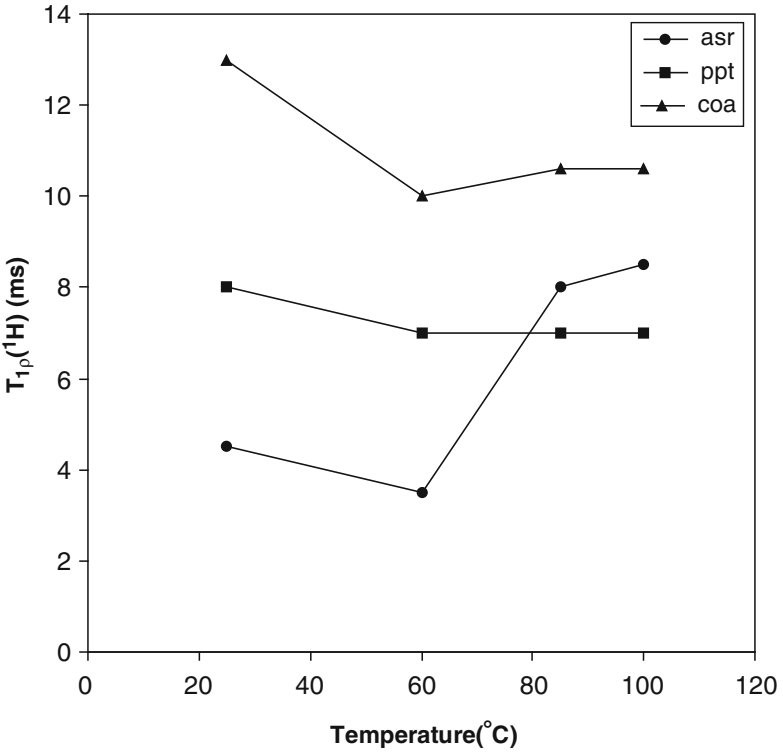

Fig. 11 Dependence of ^{1}H rotating-frame relaxation times $T^1_{1\rho}(H)$ on temperature for asr = as-received; ppt = precipitated; coa = coalesced PETs [33]

The ^{13}C-observed ^{1}H spin-lattice relaxation times observed in the rotating frame [$T_{1\rho}{}^1(H)$], which reflect motions in the kHz frequency regime, are presented as a function of temperature for our PET samples in Fig. 11. The results are consistent with the presence and absence of a glass transition observed in the DSC scans of as-received and coalesced (see Fig. 7) or precipitated [59] PETs, respectively. Thus, both macroscopic (DSC) and microscopic (NMR) observations point to the absence of a glass transition in the noncrystalline regions of coalesced or precipitated PETs. (Again details are presented as part of [33].)

In summary, microscopic and thermal observations of PET samples coalesced from their crystalline γ-CD–IC suggest crystalline characters and melt-crystallized morphologies that are different from normal samples. After coalescence of their segregated, extended chains from the narrow channels of the crystalline inclusion complex formed with host γ-CD, PET chains are much more readily crystallizable, and, locally, quickly form small, possibly chain-extended crystals. In addition, the noncrystalline regions of coalesced PET exhibit conformational and motional

behavior quite distinct from as-received PET. The extended kink conformations adopted by guest PET chains included in the PET-γ-CD–IC crystals are largely retained upon coalescence, and as such, are not only readily crystallizable, but result in the absence of normal glassy behavior for those coalesced PET chains that do not crystallize. What remains puzzling is the apparent retention of the extended kink PET conformers in the coalesced melt, even after holding it at $T > T_m$ for extended periods, and which still results in their rapid crystallization upon cooling to a distinct, possibly chain-extended crystalline morphology.

4.1.2 Polyolefins

Coalesced i-PP [42, 85–91]

Wide-angle X-ray diffractograms of as-received, precipitated, and coalesced isotactic polypropylene (i-PP), though not presented here [42], clearly indicated that only the α-form polymorph is present in the as-received and coalesced samples and a very poor α-form or almost a smectic form is obtained in the precipitated one [85–87]. Careful analysis of all diffractograms and DSC observations revealed that the γ-CD inclusion/coalescence process does not modify the crystalline form nor the melting temperature of the coalesced i-PP, but does yield a higher crystallinity for the coalesced i-PP, with an increase of about 27% in comparison with that of as-received i-PP. A significant increase in the crystallization rate from the melt was also observed for coalesced i-PP, which crystallized at 130°C compared with melt-crystallization temperatures of 117°C for as-received i-PP or 121°C for precipitated i-PP. Holding the coalesced i-PP sample in the melt at 200°C for an extended period did not alter its recrystallization behavior. Similar behavior has been observed in other semicrystalline coalesced polymers, such as PET, and can be explained by considering that the included polymer chains retain a certain degree of their extended and untangled natures even after coalescence, which facilitates their rapid crystallization.

Coalesced i-PB [42, 85–91]

X-ray diffractograms of as-received, precipitated, and coalesced isotactic poly(1-butene) (i-PB) are presented in Fig. 12. The diffractograms of both as-received and precipitated i-PB show clearly the form I polymorph (3_1 helical conformation) with the (110) reflection at 9.9°, the (300) at 17.3°, and the (220) at 20.2°(2θ). In contrast, the coalesced i-PB predominantly adopts the form II polymorph (11_3 helical conformation), along with some form III, which are normally obtained from the melt or by solution casting, respectively. The characteristic diffraction peaks of form II appear at $2\theta = 11.8°(200)$, 16.8° (220), and 18.1° (213). Form III has a strong reflection (110) at $2\theta = 11.8°$ and three weak (200), (111), and (120) reflections at $2\theta = 13.8$, 16.8, and 20.7°, respectively. Although very noisy, the peak at 13.8°

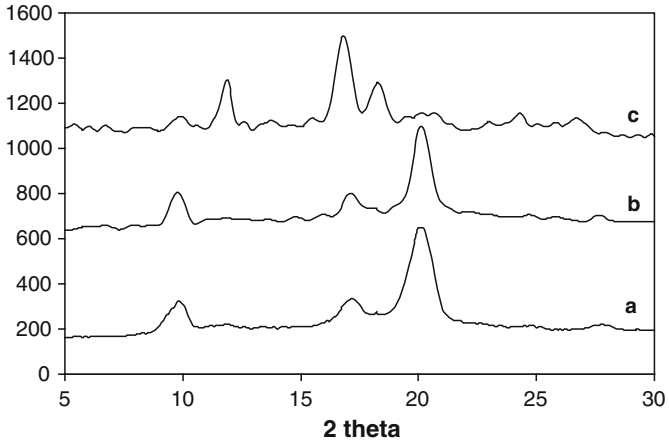

Fig. 12 WAXD patterns of as-received (**a**), precipitated (**b**), and coalesced (**c**) high molecular weight i-PB

indicates the presence of form III. The diffraction peak of form III at $2\theta = 20.7^\circ$ overlaps with a diffraction peak belonging to form I′. However, the weak peak at $2\theta = 10.0^\circ$ reveals a (110) reflection from form I or form I′. Forms I and I′ cannot be distinguished by X-rays, but exhibit different melting points in the DSC. First heating scans revealed distinct single and multiple melting peaks for the as-received and coalesced and precipitated i-PB samples, reflecting the presence of distinct crystalline polymorphs.

Interestingly, after quiescent storage for 6 months at room temperature, the coalesced i-PB, with a high molecular weight of 380,000, shows exactly the same diffraction pattern. It is very well known that the form II (tetragonal) polymorph is metastable and transforms to form I (hexagonal) at atmospheric pressure and room temperature with a half-life in the range 250–1,600 min [90]. We did not observe the same stability of the initial form II crystals when low molecular weight i-PB was coalesced from its γ-CD–IC.

As previously mentioned, CD–IC formation forces the included polymer chains to adopt an extended conformation in the host narrow channels, which in the case of i-PB might favor the formation of form I, with a more extended 3_1 helical conformation, from among its polymorphs. However, an investigation of the phase transformations in i-PB upon drawing has demonstrated [91] the formation of form II (11_3 helical conformation) upon tensile drawing and a strong dependence of the deformation process on the crystal form of the initial starting sample. Because it is likely that both form I and II helices can be accommodated in the ∼1 nm γ-CD–IC channels, these observations suggest further study of the polymorphic transformations of coalesced i-PB samples.

It is also noteworthy to mention the observation of a similar, yet even more significant, increase in the recrystallization kinetics from the melt of coalesced i-PBs

(crystallizes at 71°C upon cooling), compared with as-received or precipitated i-PBs (both crystallize at 42°C upon cooling from their melts).

4.1.3 PCL and PLLA [27]

When the biodegradable/bioabsorbable aliphatic polyesters PCL and PLLA were coalesced from their α-CD–ICs, they were observed [27] to have higher crystallinities (60 and 69% and 74 and 82% for as-synthesized and coalesced PCL and PLLA, respectively), elevated T_ms (65 and 69°C and 162 and 164°C for as-synthesized and coalesced PCL and PLLA, respectively), and, upon cooling from their melts, faster rates of crystallization and higher crystallization temperatures, T_c, than their as-synthesized counterparts. Coalescence from their α-CD–ICs is so rapid that the guest polymer chains crystallize almost at the same time they are consolidated, without losing the extended conformations required of them by the α-CD–IC channels [21]. Therefore, CD–IC formation/coalescence may be an effective way to modify the crystallinities and properties of biomedical polymers. (In this regard, see subsequent discussion of PCL-b-PLLA block copolymer behavior [20, 27], following coalescence from its α-CD–IC.)

The melting and crystallization behaviors observed for PCL and PLLA enzymatically coalesced with the alpha-amylase enzyme from *Bacillus licheniformis*, indicate that they might lead to superior drug carriers when coalesced from common CD–ICs also containing drugs (see Fig. 13). The rapid solidification of PCL

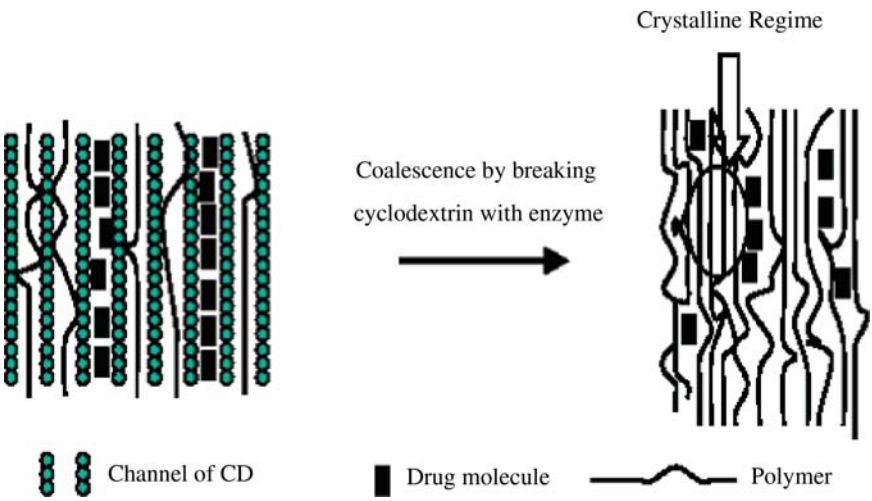

Fig. 13 Scheme of a polymeric drug delivery system formed by the simultaneous coalescence of matrix polymer and drug molecules from their common inclusion complex

and PLLA upon coalescence [12] implies a potentially improved dispersion of the drug in the PCL and PLLA matrices, which likely will critically impact their ability to deliver drugs.

4.1.4 Nylon [23, 37, 92–94]

We successfully formed an inclusion complex between nylon-6 and α-CD, and attempted to use the formation and subsequent disassociation of the nylon-6-α-CD–IC to manipulate the polymorphic crystal structures, crystallinity, and orientation of nylon-6 chains in the coalesced sample. Examination of as-received and IC-coalesced nylon-6 samples showed that the α-form crystalline phase of nylon-6 is the dominant crystalline component in the coalesced sample. X-ray diffraction patterns (Fig. 14) demonstrate that the γ-form is significantly suppressed in the coalesced sample. Along with the change in crystal form, an increase in crystallinity of ∼80% was revealed by DSC, and elevated melting and melt-recrystallization temperatures were also observed for the coalesced nylon-6 sample, in comparison to the as-received nylon-6 pellets. Thermogravimetric analysis indicated that nylon-6 has an ∼30°C higher thermal degradation temperature after modification by threading into and being coalesced from its α-CD–IC.

FTIR spectroscopy revealed a significant degree of orientation for the nylon-6 chains coalesced from their α-CD–IC crystals.In the FTIR spectrum of the IC-coalesced sample (Fig. 15), there is a very strong 1,030 cm^{-1} peak compared to

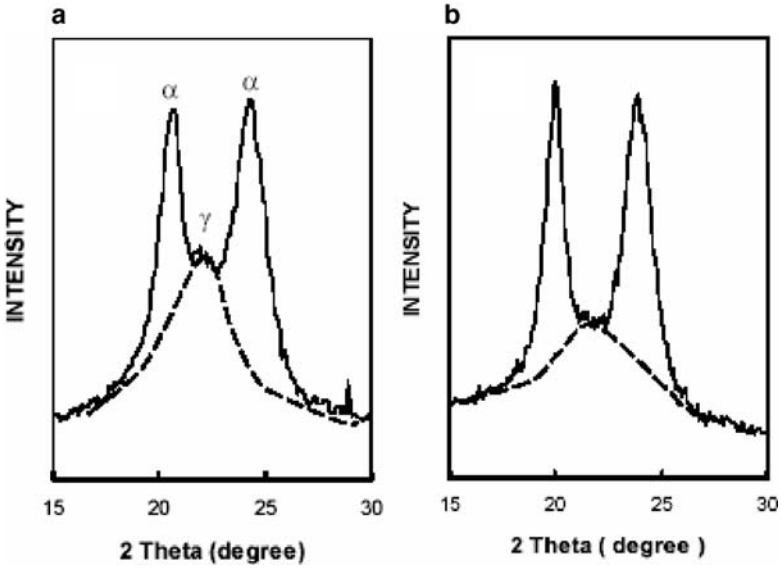

Fig. 14 Wide Angle X-ray Diffraction Patterns of (**a**) as-received and (**b**) IC coalesced nylon-6 [23, 92–94]

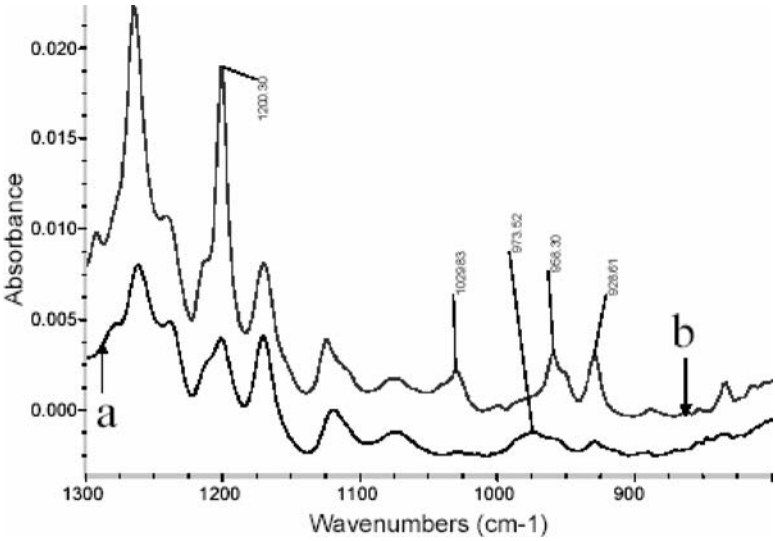

Fig. 15 Expanded FTIR spectra of (**a**) as-received and (**b**) IC coalesced nylon-6 [23, 92–94]

as-received nylon-6. According to FTIR studies of nylon 6-yarns, it is clear that the intensity of this peak increases with increasing draw ratio [95]. This may demonstrate that the extended, planar conformation that must be adopted by nylon-6 chains in the narrow channels of its α-CD–IC crystals are substantially retained after coalescence.

4.1.5 PEI [58]

The glass transition temperature of poly(ethylene isophthalate) (PEI) coalesced from its γ-CD–IC is ∼15–20°C higher (∼70°C) than that of the as-synthesized PEI, though both appear completely amorphous [58]. Typically polymer chains in amorphous regions start to move at the glass transition temperature. The coalesced PEI chains only begin to move at a temperature significantly higher than as-synthesized PEI chains, probably because the coalesced PEI chains are extended and their packing is more orderly than in the as-synthesized totally amorphous PEI with its randomly coiling chains. The greater extension and tighter packing of coalesced PEI chains apparently remains even after heating well above T_g to 260°C, because nearly identical elevated T_g s are observed during the first and second DSC heating scans. These observations somewhat parallel those observed previously for coalesced PET [21,33], where in the noncrystalline sample regions chains were also more tightly packed.

The process of coalescing PEI from its inclusion compound with γ-CD has resulted in the extension and parallelization of PEI chains during the formation of the inclusion compound, which do not completely disappear after the removal of

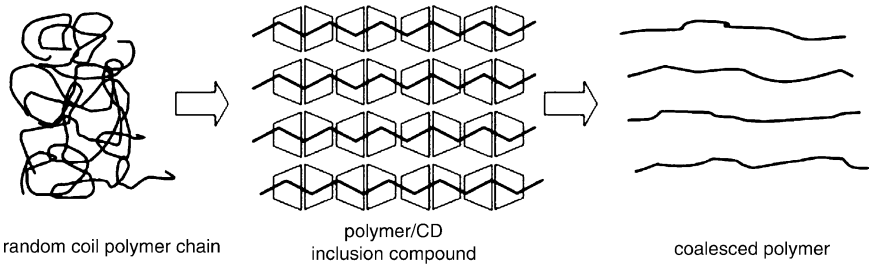

Scheme 1 Representation of polymer chain packing in PEI controlled by the formation of and subsequent coalescence from its γ-CD-inclusion compound

γ-CD by washing with hot water and coalescence of the PEI chains. A schematic representation of our view of the formation of and coalescence from PEI-g-CD–IC is shown in Scheme 1. The 15–20°C elevation in T_g of amorphous PEI produced by inclusion in and coalescence from its γ-CD–IC is significant, the more so because the coalesced amorphous PEI with tighter chain-packing does not disorder even after heating above its T_g to 260°C.

4.1.6 PVA Gels [43]

We prepared and characterized poly(vinyl alcohol) (PVA) hydrogels formed during freeze–thaw (F–T) cycles of their aqueous solutions, which also contained γ-CD [43]. Crystalline inclusion compound (IC) formation was observed between PVA and γ-CD in these gels at low concentrations of γ-CD (γ-CD:PVA molar ratios $<1:25$). Confirmation of the existence of the channel structure for γ-CD was achieved by characterizing the dried PVA/γ-CD hydrogels with solid-state DSC, TGA, WAXD, and ^{13}C-NMR. Some aspects of the mechanism of formation and structures of PVA gels obtained via F–T cycles in the presence/absence of γ-CD were presented based on UV–Vis, swelling, solution ^{1}H-NMR, and rheological observations. It was observed that the swelling and rheological responses [96–98] of the aqueous PVA gels formed during F–T cycles in the presence of γ-CD can be controlled by adjustment of the γ-CD:PVA molar ratio employed during their gelation.

Rheological observations of PVA hydrogels with γ-CD formed during five F–T cycles evidenced lower elastic moduli, G', than pure PVA hydrogels subjected to the same treatment. The magnitude of G' was a function of the quantity of γ-CD present in the hydrogels. When the concentration of γ-CD increased, G' decreased. Similarly in Fig. 16 the swelling ratio, $Q_r = \frac{W_s - W_r}{W_r}$, where the swollen and nascent sample weights W_s and W_r, respectively, of the various PVA and PVA/γ-CD gels are presented, and they are shown to increase with the increased presence of γ-CD during the F–T cycles. Both observations strongly imply that the threading of PVA chains by γ-CD, thereby isolating them and preventing their cooperative hydrogen

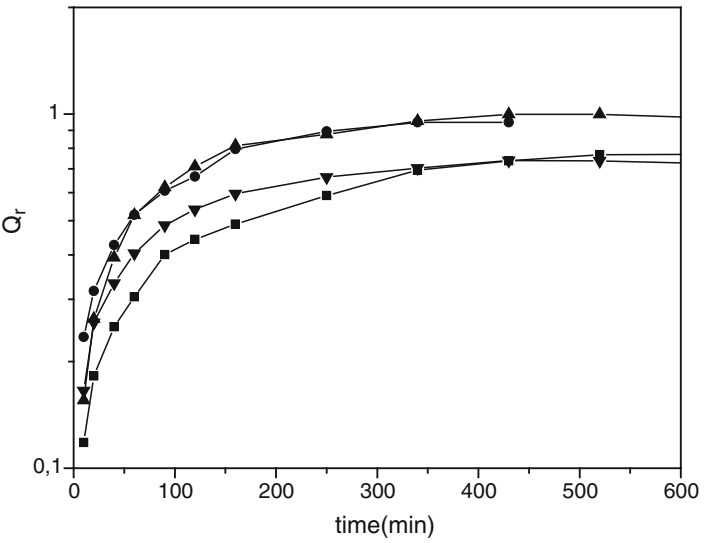

Fig. 16 Swelling measurements of PVA-γ-CD hydrogels subjected to five freezing–thawing cycles as a function of time for different PVA:γ-CD molar ratios: (*filled box*) PVA 10% ($g\,ml^{-1}$); (*filled circle*) PVA/γ-CD (26:1); (*filled triangle*) PVA/γ-CD (39.5:1); and (*filled inverted triangle*) PVA/γ-CD (53.4:1)

bonding and crystallization, limits the primary source of PVA physical cross-links in these gels [99].

According to these and other experimental results, we have proposed structures for PVA gels formed in the presence of γ-CD, which are shown in Fig. 17. As can be seen there, some small portions of the PVA polymer chains may be covered by γ-CD. Unlike the nascent and swollen gels observed as films after drying, WAXD observation of the PVA-γ-CD hydrogels show no evidence of crystallinity, so the γ-CD remaining after swelling the nascent PVA/γ-CD gels is only threaded on the PVA chains, as illustrated, or it is dissolved in the water and is removed from the gel upon swelling. In fact, ^{1}H-NMR observations of the PVA/γ-CD hydrogels performed upon dissolution in D_2O indicated that most (∼70%) of the γ-CD present in the nascent gels remains after swelling. The portions of the PVA chains that are not covered by γ-CD can presumably interact through PVA hydrogen bonds leading to the formation of the PVA/γ-CD hydrogels via freeze–thaw cycling and subsequent swelling.

Whether nascent or swollen, all of our PVA and PVA/γ-CD hydrogels were found to be soluble in D_2O indicating an absence of the formation of chemical cross-links produced by the scission of PVA chains during their F–T preparation, which had been reported previously [98]. It is clear that the elasticities of the PVA and PVA/γ-CD hydrogels studied here are a result of the physical cross-linking of PVA chains.

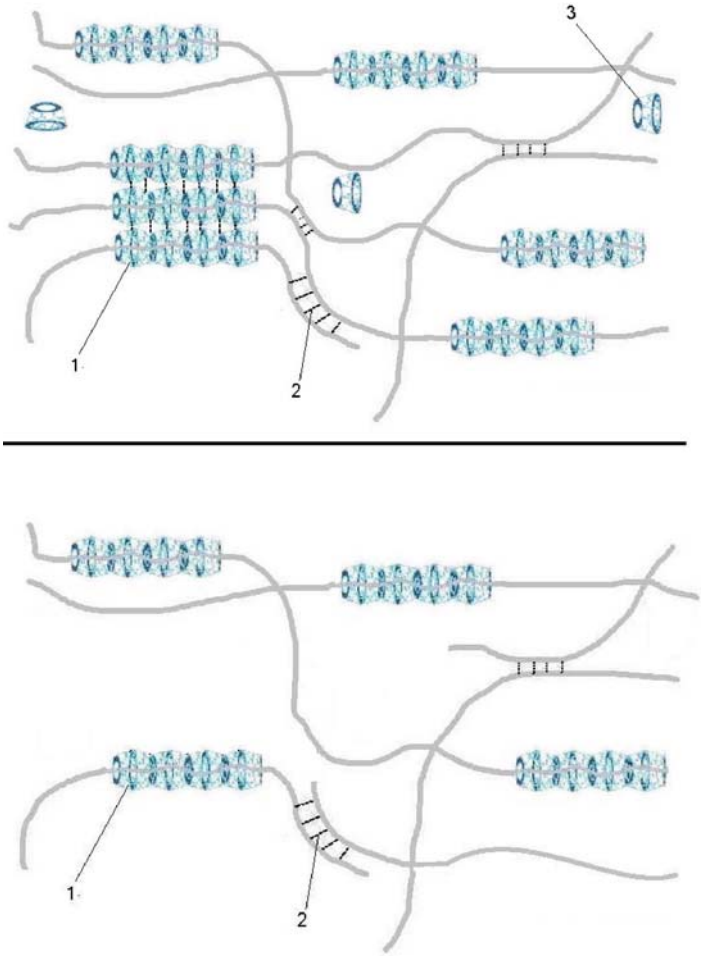

Fig. 17 Schematic illustrations of the proposed structures of PVA/γ-CD dried films (*upper*) and swollen gels (*lower*) produced by F–T cycling. **1** channel structure of PVA-γ-CD–IC, **2** hydrogen-bonded interactions/crystals/cross-links between PVA chains, and **3** free γ-CD molecules

4.1.7 Silk Protein [48]

Recently, and for the first time, we reported the formation of a CD–IC with a guest protein, silk fibroin from the *Bombyx mori* silk worm (SF) [48]. Formation of the crystalline SF-γ-CD–IC was verified by wide-angle X-ray diffraction, solid-state NMR, and infrared spectroscopy to have the host γ-CD molecules arranged in a channel structure (see Fig. 1e, f), with the extended and isolated silk chains included, at least in *large part*, in their internal cavities. Coalescence of the SF chains, by washing the γ-CD molecules away with warm water, led to suppression of the silk I and/or randomly coiling entangled conformations in the resulting solid SF sample,

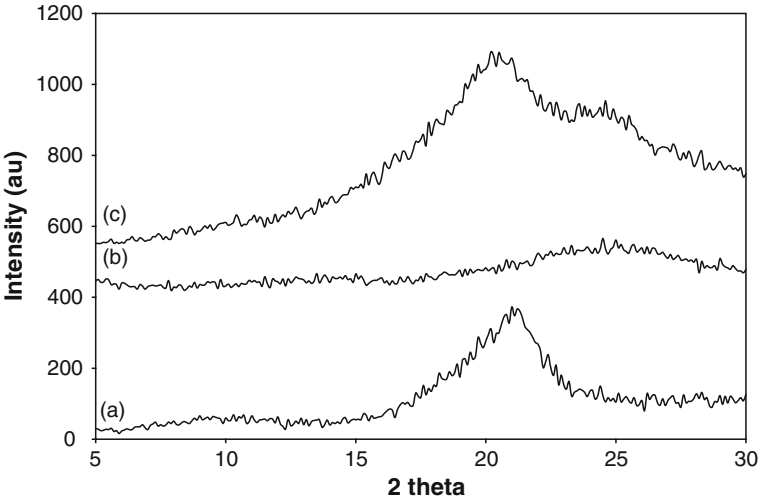

Fig. 18 Powder X-ray patterns of degummed native silk fibroin (SF) fibers from the *Bombyx mori* silk worm (**a**), SF precipitated from a $Ca(NO_3)_2 \cdot 4H_2O/2MeOH$ solution (**b**), and SF coalesced from its γ-CD–IC (**c**)

which instead contained a much higher quantity of silk-II β-sheet conformation. FTIR, WAXD, and solid-state ^{13}C NMR analyses indicated a higher degree of crystallinity and more orientated chains for the coalesced SF in comparison with the precipitated SF sample, as may be seen in Fig. 18, much like the initial degummed SF fibers. Note the preponderance of silk-II (scattering peak at $2\theta = 21^\circ$ from the β-sheet structure) in both the degummed native fiber and coalesced SF samples, while scattering at $2\theta = 25^\circ$ from silk-I preponderant in the precipitated sample is minimal in the coalesced sample. These modifications may have a substantial impact on the overall physical properties of γ-CD-processed silk. As a consequence, γ-CD–IC formation/coalescence processing has proved to be an effective method of manipulating both the polymorphic structures and the final level of crystallinity in the SF protein, mimicking the actual spinning behavior of the silk worm.

Though ∼85% of the amino acid residues in the SF protein are compact with small side chains (glycine, alanine, and serine), near both the N- and C-termini of the SF chain, several quite bulky amino acid residues (proline, histidine, trypthophan) are present in the SF primary structure [100]. At first glance, the possibility that γ-CDs (9–10Å channel diameter) have completely threaded over SF protein chains to form the SF-γ-CD IC seems unlikely. However, there is precedence for such an observation in the study of the complexation of propylene oxide-*b*-ethylene oxide-*b*-propylene oxide (PPO–PEO–PPO) block copolymer with α-CD [101]. As pointed out in this study, PPO and PEO homopolymers are known to form CD–ICs only with β- and α-CDs, respectively. Nevertheless, it was observed there that α-CDs are able to thread over the bulkier PPO end-blocks and complex with the central PEO

block. In an analogous manner, γ-CDs are apparently able to thread over the bulky amino acid residues in the SF protein chains and form a SF-γ-CD–IC [75].

4.2 Nonstoichiometric Polymer-CD–ICs as Nucleating Agents for the Crystallization of Polymers [103–106]

Formation of polymer-CD–ICs with amounts of host CDs insufficient to completely thread and confine the guest polymers, results in polymer-CD–IC crystals with portions of the guest polymer chains emerging from the host CD crystalline surfaces [102]. When a nonstoichiometric (*n-s*) polymer-CD–IC, with only partially included chains, is added in small quantities to a bulk sample of the same polymer, which can crystallize and has a T_m below the decomposition temperature of CD–ICs ($\sim$ 250–300°C), it has been observed that its crystallization from the melt is enhanced [103–106]. Melt crystallized polymers nucleated with *n-s* polymer-CD–ICs crystallize more rapidly, evidence greater levels of crystallinity, higher melt crystallization temperatures, and semicrystalline morphologies characterized by crystals which are smaller and more uniformly distributed than in un-nucleated pure bulk samples.

The effectiveness/efficiency of nucleation with (*n-s*) polymer-CD–ICs was observed to be at least comparable or superior to that produced by more traditional nucleation agents, such as talc, and for that matter pure CDs. The alteration of crystalline morphology achievable by using *n-s* polymer-CD–ICs as nucleants in melt-crystallization is demonstrated in Fig. 19. It is very clear that the morphology of PCL melt-crystallized in the presence of a small amount of (*n-s*) α-PCL-C–IC is very distinct from the pure melt-crystallized PCL. Crystal sizes are drastically reduced and more homogeneously distributed for the nucleated PCL.

The distinct changes in morphology achieved by melt-crystallization of polymers in the presence of small amounts of their (*n-s*) polymer-CD–ICs results in changes in other physical properties as well. For example, in Table 2 a comparison of the properties of poly(3-hydroxy butyrate) (PHB) melt-spun with and without the presence of (*n-s*) PHB-α-CD–IC are compared [104]. The mechanical properties of the PHB/(*n-s*) PHB-α-CD–IC fibers are superior. In fact, their lower elongation at break likely contributes to the removal of the stickiness normally observed between melt-spun PBH fibers [104].

There is an important additional advantage of using (*n-s*) polymer-CD–ICs to nucleate the melt-crystallization of polymers. Because CDs are nontoxic, biocompatible, and biodegradable, they may be safely utilized in (*n-s*) polymer-CD–IC nucleants to fabricate both permanent and biodegradable/bioabsorbable implants that are also nontoxic.

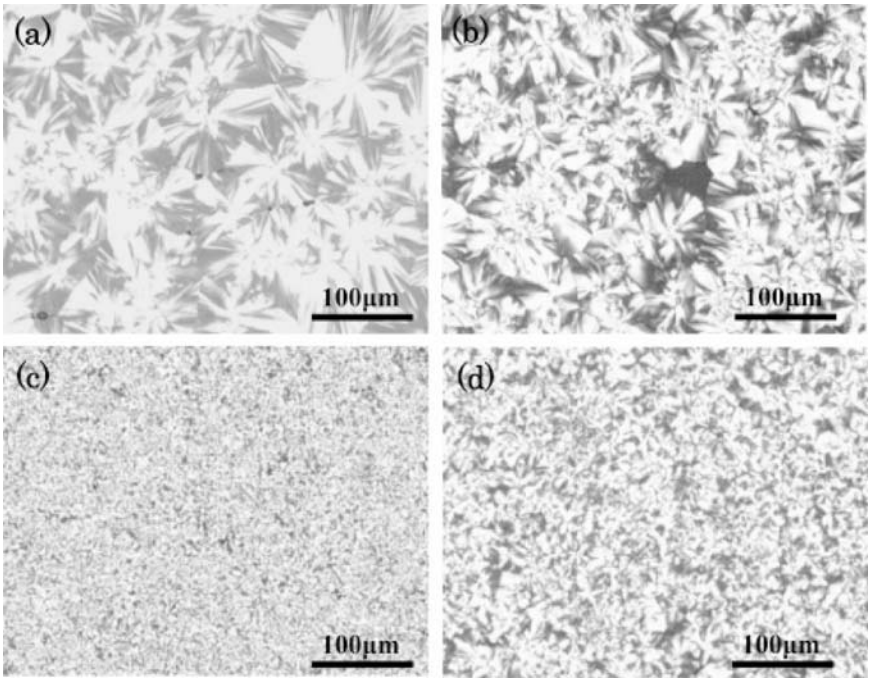

Fig. 19 Polarized optical micrographs of PCL (**a**), and PCL containing 2 wt% α-CD (**b**), talc (**c**), and (n-s) PCL-α-CD–IC (**d**) [105]

Table 2 Young's modulus, E_t, tensile stress at break, ς_H, and elongation at break, ε_H, of PHB fiber samples [104]

Fiber sample	E_t [Gpa]	$\sigma_H[N-mm^{-2}]$	ε_H [%]
PHB (DR 3)*	4.45	116.64	50.02
PHB (DR 4)	4.44	164.38	52.82
PHB + 0.5% IC	4.94	161.33	18.51

*Draw ratio

4.3 Homopolymer Blends Coalesced from their Common CD–ICs

By combination of a solution containing two chemically distinct dissolved polymers with a CD solution, it is possible to form a common CD–IC containing both guest polymers. Assuming that each of the guest polymers is randomly included or "mixed" in the CD channels of their common CD–IC (see Figs. 1f, 2), we may anticipate that upon coalescence an intimate blend would result. The intimate blending of normally incompatible polymers, both binary and ternary blends, by coalescence from their common CD–ICs has in fact been demonstrated [40].

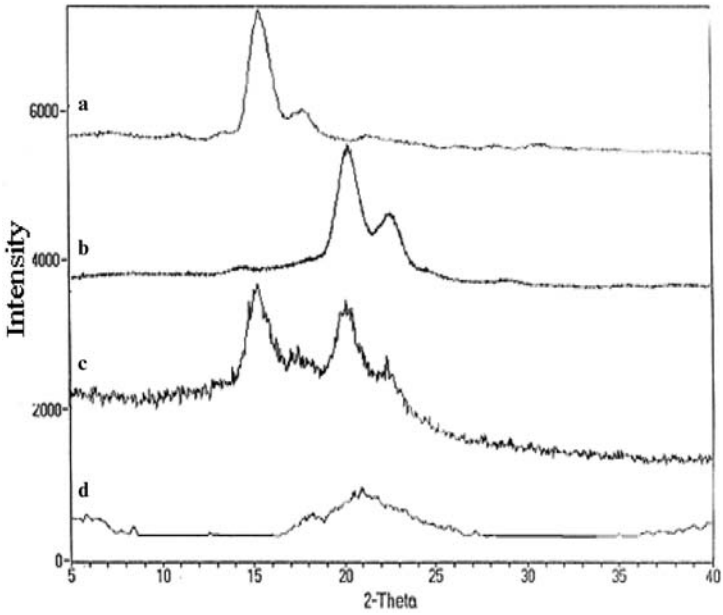

Fig. 20 X-ray diffractograms of pure PCL (**a**) and PLLA (**b**) and PCL/PLLA blends obtained by casting from dioxane solution (**c**) and hot water coalescence from PCL/PLLA-α-CD–IC (**d**) [12]

4.3.1 PCL/PLLA Blends [12, 27, 46]

In Fig. 20 the X-ray diffractograms of the biodegradable/bioabsorbable polyesters PCL, PLLA, and their blends, either cast from dioxane solution or coalesced from a common α-CD–IC containing both PCL and PLLA as guests, are presented. Their solution-cast blend shows extensive crystallinities for both phase-segregated components, while the PCL/PLLA blend coalesced from their common α-CD–IC crystals shows virtually none and very little PCL and PLLA crystallinities, respectively. Unlike the solution-cast blend, the mainly amorphous coalesced blend strongly suggests intimate mixing of PCL and PLLA chains, which prevents their separate crystallization. In fact detailed analyses of two-dimensional HETCOR NMR spin-diffusion experiments [46] revealed that the length scale of mixing in the coalesced PCL/PLLA blend is smaller than the radii of gyration of both components and the mobility of PLLA chains in this blend is greater than in the amorphous regions of pure PLLA. Both observations confirm that PCL and PLLA chains are indeed intimately mixed in the blend coalesced from their common α-CD–IC crystals.

4.3.2 PVAc/PMMA Blends [40, 47, 49, 51]

Direct insertion probe mass spectrometry (DIP–MAS) analyses of poly(methyl methacrylate) (PMMA), poly(vinyl acetate) (PVAc), and their coalesced and precipitated blends were performed [51] (see Fig. 21). The fact that the pyrolysis mass

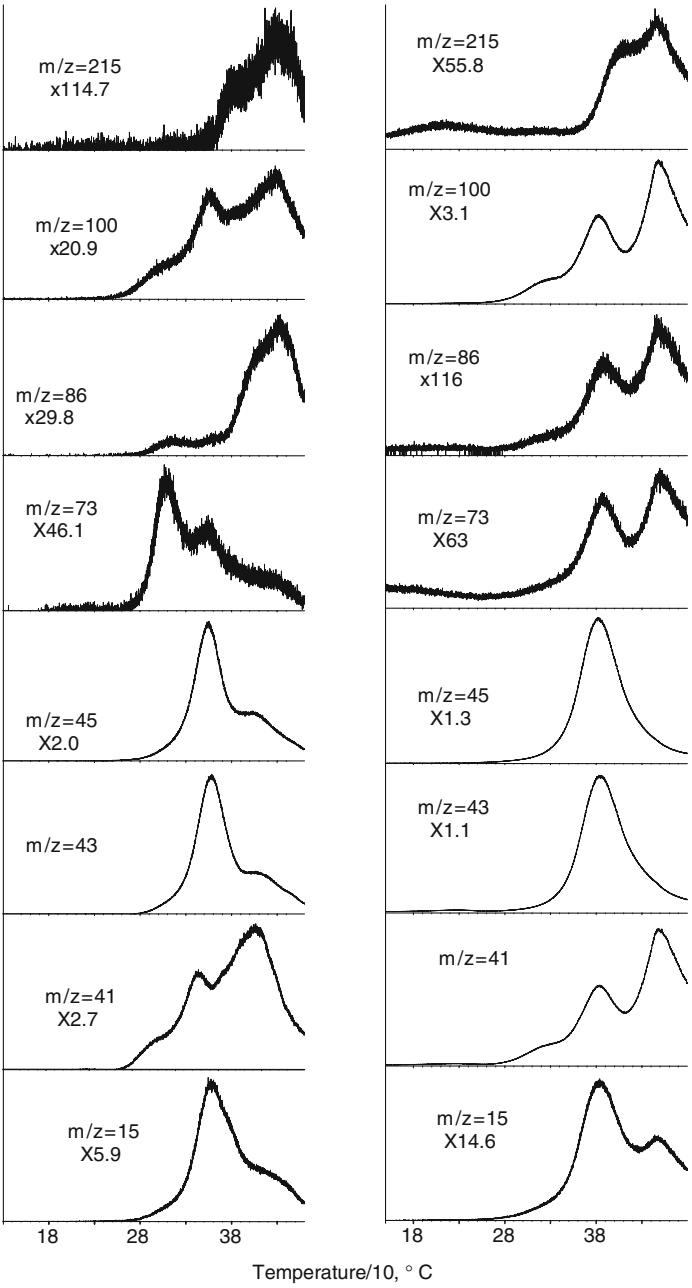

Fig. 21 Evolution profiles of some characteristic products recorded during the pyrolysis of the coalesced (*left*) and solution-cast (*right*) PMMA/PVAc blends

spectra of all the samples were dominated by peaks having the same m/z values, though they were due to different thermal degradation products, caused some additional difficulty in the analyses of PMMA/PVAc physical and coalesced blends. To reach reliable conclusions more emphasis was given to the trends in the evolution profiles of their thermal degradation products.

PVAc degrades in two stages, around 360 and 440°C, corresponding to deacetylation and disintegration of the polyolefinic backbone, respectively. For PMMA the low temperature weight losses were attributed to evolution of dimer, low molecular weight oligomers, scission of head-to-head linkages, and loss of unsaturated end groups. At elevated temperatures (380–420°C), however, initiation of weight loss was thought to be a mixture of chain end and chain scission processes, followed by depropagation to the end of the polymer chain. It is known that the probability of cleaving a particular bond during thermal degradation depends not only upon its inherent strength, but also on the stability of products formed.

It is clear that the thermal degradation behaviors of both PVAc and PMMA have been changed in the coalesced blend. The decrease in MMA monomer yield may be associated with inhibition of PMMA depolymerization. Depolymerization of PMMA can be inhibited if the loss of side chains is favored, which implies that proton-transfer to the C = O groups of PMMA occurs. So, for the coalesced PMMA/PVAc blend, PMMA depolymerization was likely inhibited as a result of proton-transfer to the C = O groups of the MMA units. Because both coalesced and as-received PMMA degrade mainly by depolymerization reactions, the source for the depolymerization inhibiting proton transfer in the coalesced blend could only be PVAc. However, it is clear that the simple presence of PVAc was not sufficient for proton-transfer, as depolymerization of PMMA was also recorded for the phase-segregated PMMA/PVAc physical blend. Instead, it may be suggested that such a proton-transfer can only be possible if the separation between PMMA and PVAc chains is comparable to the distance between γ-H and C = O groups within a single PMMA molecule.

It seems likely that PVAc containing CH_3–C = O groups, with more acidic protons, should be more effective in McLafferty-type rearrangement reactions and intermolecular proton-transfer to PMMA chains, even if the distances between PVAc–PMMA and PMMA–PMMA are comparable, i.e., PMMA and PVAc chains in the coalesced blend are very intimately mixed. Making use of the above proposal permits the approximate reaction scheme shown in Scheme 2 to be written.

As a result of such an intermolecular proton-transfer from PVAc to PMMA, the thermal degradation of PVAc should shift to the high temperature ranges. Furthermore, thermal degradation products of poly(methyacrylic acid) (PMA) should appear in the pyrolysis mass spectra. Because of the similarities in the structures of PMMA and PMA, a depolymerization reaction yielding mainly CH_2CCH_3COOH, CH_2CCH_3, and COOH fragment peaks at $m/z = 86, 43$, and 45 Da, respectively, can be expected. The pyrolysis data indicating an increase in relative intensities of the 15 Da peak (due to CH_3), in the temperature range where PVAc degrades, and the 45 and 86 Da peaks (due to COOH and CH_2CCH_3COOH, respectively), in the temperature region where PMMA degradation occurs, support the proposed

intermolecular proton-transfer from PVAc to PMMA in the coalesced blend. The relative intensity ratios of the above-mentioned peaks in the pyrolysis mass spectra are summarized in Table 3.

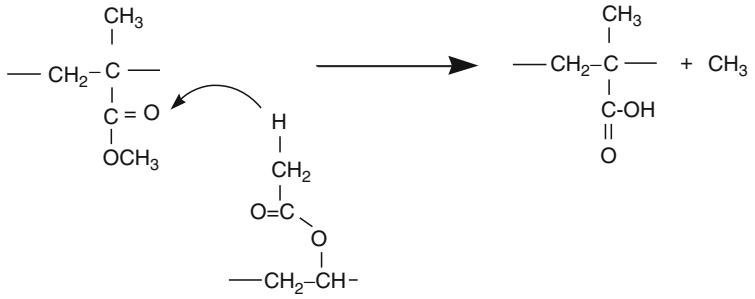

Scheme 2 Proposed McLafferty-type rearrangement via intermolecular proton transfer from the CH_3 of PVAc to the ester group of PMMA in the well-mixed coalesced PVAc/PMMA blend. Note that only the conversion of PMMA to PMA is depicted in the proton-transfer from PVAc

Table 3 The assignments and intensities (relative to the weakest peak) of the characteristic and intense peaks in the pyrolysis mass spectra of physical and coalesced PMMA/PVAc blends at temperatures corresponding to maxima in the TIC curves (Fig. 21) [51]

m/z, Da	PMMA/PVAc 360°C	Physical mixture 430°C	Coalesced 310°C	PMMA/PVAc 360°C	430°C	Assignments
15	75	46	80	152	151	CH_3
41	585	1,000	1,000	276	1,000	CH_2CCH_3
43	1,000	207	979	1,000	725	CH_2CHO, CH_3CO
45	769	115	505	509	352	COOH, CHOO
60	690	85	566	300	195	CH_3COOH
69	546	924	649	141	544	CH_2CCH_3
73	13	17	241	16	20	$C_3H_5O_2$
78	103	14	22	63	49	C_6H_6
86	6	8	37	3	77	$C_4H_6O_2$, VAc
91	46	51	73	26	164	C_7H_7
100	215	351	140	39	116	MMA
128	51	42	36	24	83	$C_{10}H_8$
141	25	37	26	8	58	$C_{12}H_9$
179	15	38	25	7	31	$C_{14}H_{11}$
180	13	13	5	6	21	$C_{14}H_{12}$
215	6	16	21	3	24	$C_{14}H_{12}$
232	3	5	4	2	8	$C_{18}H_{16}$
284	1	2		1	4	$C_{22}H_{20}$
315	1	3		1	7	$C_{24}H_{27}$

4.3.3 PC/PMMA/PVAc Ternary Blends [35]

We reported the formation of an intimate polycarbonate (PC)/PMMA/PVAc ternary blend by coalescence of these polymers from their common IC formed between γ-CD hosts and PC, PMMA, and PVAc guests [35]. Figure 22 shows the MDSC thermograms of the ∼1:1:1 molar coalesced PC/PMMA/PVAc ternary blend. The total signal of heat flow may be separated into reversing and nonreversing heat flows, as a result of the temperature modulation employed. Thermal transitions in the reversing signal arise from thermodynamic phenomena, such as the T_g and melting. The nonreversing signal exhibits kinetic phenomena, including evaporation and recrystallization. By plotting the reversing heat flow versus temperature, the effect of the solvent release, as well as enthalpic recovery (an endothermic peak that occurs just above the T_g), are eliminated, revealing a clear, single glass transition.

In both the first and second MDSC heating scans, only a single glass transition can be observed at 57°C, which is different from the glass transition temperatures observed for pure PC (133°C), PMMA (82°C), and PVAc (39°C) by DSC in Fig. 23 for the phase-segregated PC/PMMA/PVAc blend coprecipitated from their common solution. This result indicates the presence of a single homogeneous amorphous phase in the coalesced ternary blend of PC/PMMA/PVAc, where the three component polymer chains are intimately mixed with each other. The appearance of one glass transition in the second scan also confirms the stability and molecular degree of mixing of the PC, PMMA, and PVAc chains in their coalesced blend. The

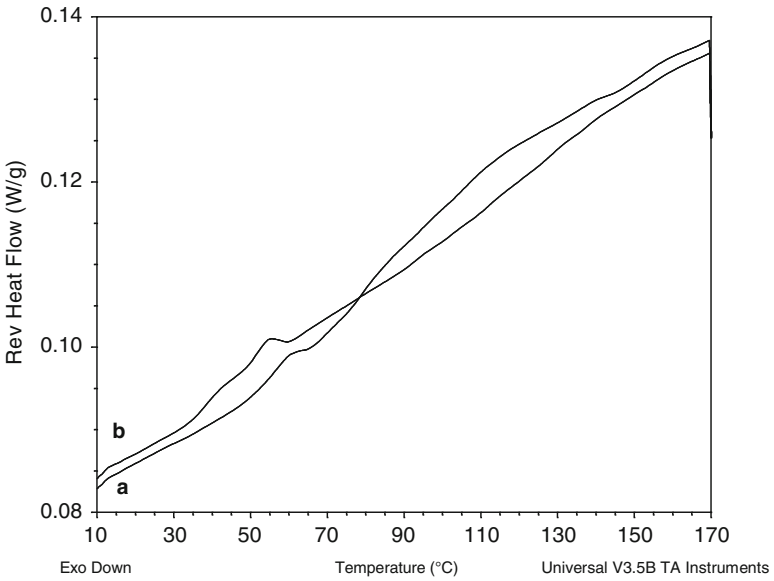

Fig. 22 MDSC scans of the (**a**) first, and (**b**) second heating runs recorded for the ∼1:1:1 molar PC/PMMA/PVAc coalesced blend. The sample was held for 3 min at 170°C after the first heating [35]

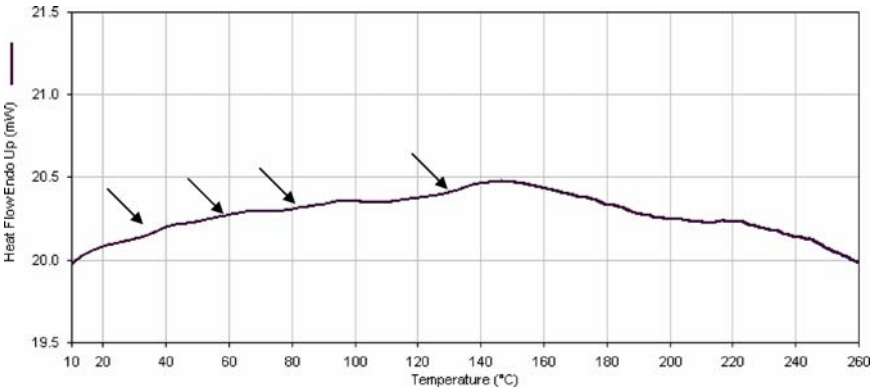

Fig. 23 DSC thermogram of the coprecipitated PC/PMMA/PVAc blend, first heating scan

DSC scans recorded for PC/PMMA/PVAc blends obtained by solvent-casting and coprecipitation evidenced four distinct glass-transitions, one for each component polymer and one indicating that some of the PMMA and PVAc chains were mixing (see Fig. 23).

We also observed that the PC chains possess a preferred ability to form inclusion compounds with γ-CD in solution, when competing with PMMA and PVAc. From the ^{1}H NMR spectrum of the coalesced ∼1:1:1 PC/PMMA/PVAc blend (not shown), the molar ratio of PC:PMMA:PVAc was determined to actually be 1.6:1:1.4 compared to the initial molar ratio of 1:24:24, respectively, used in solution to form their common γ-CD–IC. Despite the initial 1:24:24 PC:PMMA:PVAc molar ratio in solution, the PC component in the coalesced PC/PMMA/PVAc blend is still prevalent over the PMMA and PVAc components, which indicates that there may be additional factors that govern the inclusion process from a multiguest system. We believe that this very strong preference of the host γ-CD molecules for PC chains, rather than the other two possible guests, is due to their different hydrophobicities. Although the final molar ratio of the coalesced ternary blend can be somewhat controlled by modifying the initial molar ratio of polymers in their common solution, our eventual aim is to be able to adjust, as desired, the constituent polymer ratios in coalesced ternary blends.

4.4 Coalescence of Block Copolymers from their CD–ICs

Inherently incompatible blocks in block copolymers normally segregate into separate phases in the bulk. However, if block copolymers are included in and then subsequently coalesced from their CD–ICs, the phase segregation of their incompatible blocks may be controlled. For example, if all blocks of a block copolymer are included in its CD–IC, then, similar to the case for common CD–ICs containing two or more homopolymers, upon coalescence we would expect a reduction in the phase segregation of their blocks. On the other hand, if some blocks are included

in their CD–ICs, while others are not, then we might anticipate an increased phase segregation of their constituent blocks upon coalescence.

4.4.1 PCL-b-PLLA [18, 20, 27]

When melt-pressed films of as-synthesized PCL-b-PLLA and PCL-b-PLLA that had been included in and then coalesced from its α-CD–IC are observed by X-ray diffraction (see Fig. 24) [20], it is clear that the coalesced film is predominantly amorphous, as a consequence of the mixing of PCL and PLLA blocks, while the as-synthesized PCL-b-PLLA film shows substantial crystallinity for both the PCL and PLLA blocks (compare with Fig. 20), indicating a phase segregation of blocks. These PCL-b-PPLA films were then subjected to enzymatic degradation and their structures monitored with X-ray diffraction. From Fig. 24 we can see that the phase segregated as-synthesized block copolymer film underwent only limited degradation even after 2 weeks of enzymatic digestion. The coalesced PCL-b-PLLA film on the other hand experienced much more extensive degradation, as evidenced by the transition of its X-ray diffraction pattern from that of a largely amorphous material initially to one that is highly crystalline after 14 days of degradation. Clearly the enzyme almost exclusively attacked the abundant amorphous sample regions of the coalesced film, where the PCL and PLLA blocks are well mixed. Thus, the biodegradation of block copolymers, and by extension, homopolymer blends can be controlled by processing them with CDs.

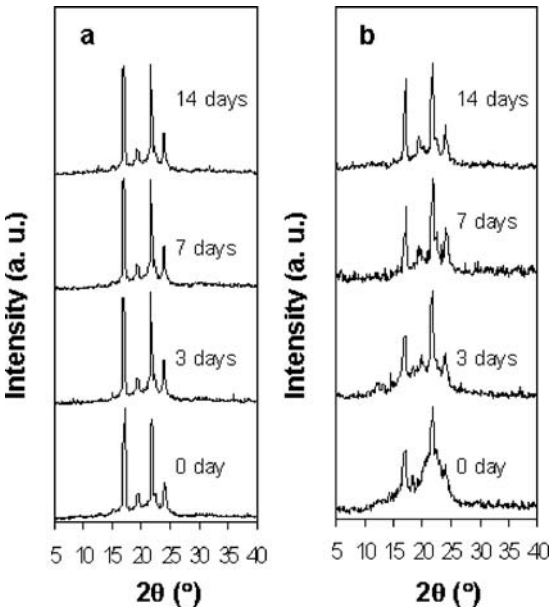

Fig. 24 X-ray diffraction patterns of as-synthesized (**a**) and coalesced (**b**) PCL-b-PLLA melt-pressed films observed following various enzymatic degradation times [20]

Table 4 Thermal properties and crystallinities, χ_c, of various PCL–PPG–PCL triblock copolymer samples revealed by DSC [25]

Sample	T_m [°C]	ΔH_m [J/g]	χ_c [%]
As-synthesized copolymer	57.3	58.6	56.5
Coalesced from α-CD–IC	63.8	76.8	74.1
Coalesced from γ-CD–IC	63.0	51.3	49.5

4.4.2 PCL–PPG–PCL [25]

When ICs are formed between guest PCL-poly(propylene glycol) (PPG)-PCL triblock copolymer and α- and γ-CD hosts [25], in the first case only the PCL blocks are included, while in the PCL–PPG–PCL-γ-CD–IC entire triblock copolymer chains are included. As a result, in comparison to the as-synthesized triblock copolymer, we would expect that upon coalescence from the PCL–PPG–PCL-α- and γ-CD–ICs an increase and a decrease in the phase segregation of PCL and PPG blocks would occur, respectively. As can be seen in Table 4, these expectations are in fact realized as indicated by the increased, decreased level of PCL block crystallinity in PCL–PPG–PCL coalesced from its α-,γ-CD–ICs. Because two side-by-side PCL blocks may be included in the channels of the γ-CD– IC [107,108], while only single PPG blocks may be included, the less than expected minor reduction in the phase segregation achieved upon coalescence from the PCL–PPG–PCL-γ-CD–IC can be understood.

It should also be mentioned that block copolymers, such as PCL–PPG–PCL, may be utilized to form polymer-CD–ICs [102–104] that are effective as nucleating agents. For example, if β-CD is used to form an IC with PCL–PPG–PCL, only the central PPG blocks will be included [101], and the unincluded terminal PCL blocks will extend from the surfaces of the b-PPG-β-CD–IC crystals. By altering the PCL block lengths we may be able to tailor their ability to control the melt-crystallization of PCL. In comparison to $(n\text{-}s)$ PCL-α-CD–ICs, or $(n\text{-}s)$ polymer-CD–ICs in general, block copolymer-CD–ICs with some blocks able to be included, while other blocks are excluded, may potentially be superior nucleating agents.

5 Additive CD complexes

It is possible to more effectively deliver small-molecule additives to polymers by employing either crystalline additive-CD–ICs or additives that are permanently complexed/rotaxanated with CDs and that remain soluble. Additive-CD–IC complexes may be delivered by melt-processing up to temperatures of ~ 300°C, while the permanently threaded and soluble additive-CD–rotaxanes can be delivered from their solutions.

5.1 Additive-CD–ICs [7, 9, 13, 17, 52, 53, 65, 69, 70]

5.1.1 Antibacterial-CD–ICs

Because crystalline CD–ICs are high-melting and thermally stable, even when containing small-molecule guests that are volatile liquids [52, 53] or even gases in the bulk, delivery of additives to polymer materials can be improved by using additive-CD–ICs, which may often be conveniently melt-processed into polymers. An example of CD–IC delivery of a polymer additive is provided by the commercial antibacterial triclosan [17].

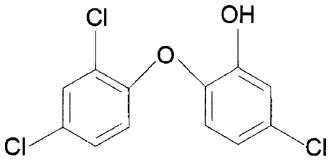

The triclosan-β-CD–IC was formed and small amounts were mixed with PCL powder, which was sprinkled onto cotton fabric and then covered with another piece of cotton fabric. The cotton-PCL/triclosan-β-CD–IC-cotton was ironed into a laminate, placed on an Agar plate, and then tested against the growth of *E. coli* bacteria. As can be seen from the test results in Table 5, *E. coli* bacteria were unable to grow upon the laminated cotton fabric containing triclosan-β-CD–IC. In fact the laminated fabric was just as effective as films of PCL containing triclosan-β-CD–IC or pure triclosan.

The use of triclosan-β-CD–IC to deliver the antibacterial properties of triclosan has an important advantage over the pure antibacterial agent. Triclosan is crystalline, but melts in the range of 55–60°C. Though it is possible to blend pure triclosan with low melting polymers like PCL ($T_m \sim 60$°C), this would not be the case for polymers with higher melting or softening temperatures. On the other hand,

Table 5 *E. coli* test results for cotton fabric laminated with PCL films embedded with Triclosan or Triclosan-β-CD–IC [17]

Sample	Zone of inhibition (diameter in mm)
PCL (between pieces of fabric) (1 g of PCL)	0
PCL (1 g of PCL)	0
PCL + triclosan (between pieces of fabric) (1 g of PCL and 0.1 g of triclosan)	15
PCL + triclosan (1 g of PCL and 0.1 g of triclosan)	15
PCL + triclosan-β-CD–IC (between pieces of fabric) (1 g of PCL and 0.1 g of triclosan-β-CD–IC)	12–15
PCL + triclosan-β-CD–IC (1 g of PCL and 0.1 g of triclosan-β-CD–IC)	14–17

triclosan-β-CD–IC is thermally stable and solid well above 250°C [53, 69, 70], and so may be melt-processed into many polymeric materials. The thermal stabilities [53, 69, 70] of small-molecule-CD–IC crystals has permitted us to more conveniently and effectively deliver [7, 9, 13, 17, 52, 53, 65, 69, 70] several additives to polymer materials, including antibacterials, flame retardants, spermicidals, and insect repellants.

5.1.2 Spermicide-CD–IC [69, 70]

A crystalline IC has been formed with α-CD and the liquid spermicide Nonoxynol-9 (N-9). Testing of siloxane rubbers embedded with small amounts of N-9-α-CD−IC

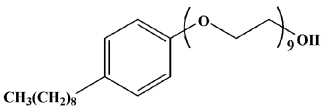

crystals against bovine sperm has begun with initially promising results (see Table 6) [69, 70]. The siloxane networks swollen with neat nonoxynol-9 and embedded with N-9- α-CD–IC crystals with similar N-9 concentrations appear to be equally effective in killing bovine sperm. However, the delivery of N-9 by embedding the rubber network with N-9-α-CD− IC crystals has two advantages over swelling the network with neat N-9: (1) more convenient and longer lasting delivery and (2) less potential for human contact with N-9. Both of these advantages are a result of the inclusion of N-9 in the crystalline matrix of its IC formed with α–CD.

Table 6 Bovine sperm motility on various silicone rubber films swollen or embedded with pure N-9 or N-9-α-CD–IC

Treatment group	wt% N-9	Sperm motility (% motile) at time [min]			
		0	10	30	60
1. Silicone rubber with N-9	0.37	26.67	2.33	0.00	0.00
2. Silicone rubber	0	41.67	40.00	21.67	8.67
3. Silicone rubber with N-9-α-CD–IC	0.44	26.67	1.67	0.00	0.00
4. Silicone runner with N-9-α-CD–IC	0.83	28.33	4.00	0.00	0.00
5. Silicone rubber with N-9	0.73	38.33	10.67	0.33	0.00
6. Silicone rubber with N-9	4.35	0.00	0.00	0.00	0.00
7. Blank well with a parafilm circle inserted	-	46.67	17.32	18.33	8.67
Untreated	-	46.67	40.00	41.67	31.67

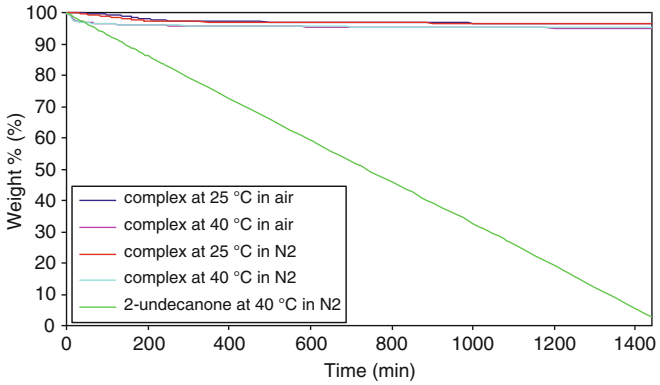

Fig. 25 Time-dependent, constant-temperature TGA scans of pure and α-CD complexed 2-undecanone

5.1.3 Insect Repellant-CD–IC [69, 70]

2-Undecanone (methyl nonyl ketone), a natural nontoxic insect repellant compound, was recently isolated from the trichomes of wild tomatoes, and is currently being introduced as a replacement for insect repellants containing N,N-diethyl-meta-toluamide or DEET, which are permitted for use only on children older than 2 months. In an effort to improve the delivery of the somewhat volatile liquid 2-undecanone, we have successfully formed the crystalline inclusion compound (IC) between 2-undecanone and α-CD, using a coprecipitation method [69, 70].

The release characteristics of 2-undecanone insect repellant from its α-CD–IC were studied using TGA either at a heating rate of 20°C/min in nitrogen and air atmospheres or at constant temperatures of 25 and 40°C over a period of 24 h (see Fig. 25). By integrating and comparing the areas of resonance peaks contributed by 2-undecanone and α-CD in the ^{1}H NMR spectrum of 2-undecanone-α-CD–IC, it was found that α-CD forms a 2:1 inclusion complex with 2-undecanone. This translates to 8 wt% 2-undecanone and 92 wt% α-CD in the stoichiometric 2-undecanone-α-CD–IC, which can be used to analyze TGA results to determine 2-undecanone weight loss.

The release/loss of 2-undecanone insect repellant from its α-CD–IC was ∼60% after 24 h at 40°C. By comparison, ∼97% of pure 2-undecanone was volatilized and lost over 24 h at 40°C. These results suggests that the gradual, long-term delivery of the insect repellant 2-undecanone can be significantly improved through employment of its crystalline α-CD–IC, as was recently demonstrated [69, 70].

5.1.4 Flame Retardant-CD–IC [13]

We successfully formed an inclusion compound (IC) between a commercial flame retardant (FR = Antblaze RD-1) [13], which is shown below in its protonated form, and β-cyclodextrin (CD). The FR-β-CD–IC was melt-processed into PET films which were tested for flammability. The flammabilities of pure PET films, PET

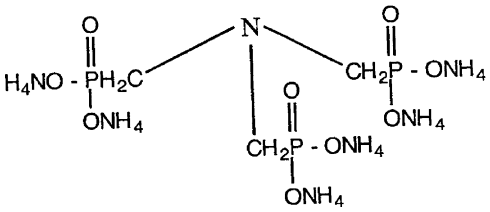

Table 7 Flammability of PET Films

	Char Length (cm)			Burning Time (s)		
Film/Trial	1	2	3	1	2	3
PET	BEL*	BEL	BEL	26.0	28.0	25.0
PET/FR	5.3	BEL	BEL	14.0	16.0	16.0
PET/β-CD	BEL	BEL	BEL	15.0	19.0	15.0
PET/FR IC	1.0	0.8	1.0	6.0	4.0	6.0

* BEL, burned entire length

films containing pure CD, and PET films containing FR applied from a bath and then oven-cured, were also observed. Flammability was measured using a modified AATCC Test Method 34, and the results are presented in Table 7. It is apparent that all but the PET films embedded with FR-β-CD–IC were either completely or substantially consumed when ignited on a single edge with a 3.8 cm flame applied for 3 s. To our knowledge, this is the only reported demonstration of flame retardance achieved by means of delivering a FR to a polymer in the form of its CD–IC.

When embedded in thin PET films at levels (10 wt%) comparable to those achieved in cotton/polyester blend fabrics via bath padding and oven-curing ($\sim$ 4–12 *wt%*), substantial flame retardancy is imparted to the PET films. This despite the fact that the molecular weights of FR and β-CD are 401 and 1,135, respectively, which suggests that the FR is actually present at much reduced levels in the FR-β-CD–IC embedded PET films.

The temperature stability of the FR-β-CD–IC crystals makes them suitable for embedding in a variety of polymers that melt below $\sim$300°C. Our results suggest that incorporation of FR-CD–ICs directly into polymer films or fibers during their melt-processing may be a means to protect them from burning that is superior to postfabrication application of FRs. In addition, liquid FRs and other additives, which are difficult to incorporate and retain in solid polymers, may be included in their high-melting ICs formed with CDs and embedded directly into polymer samples, because the guest additive is protected both from the environment and its processing into polymers by the thermally stable crystalline lattice provided by the host CD.

These results give further impetus to our belief that a variety of additives may be more effectively delivered to polymer films and fibers as high melting inclusion compounds formed with CDs. In this connection for flame retardants, which can be toxic and mutagenic on contact, their confinement in CD–ICs not only protects them from the environment, but protects the wearer of fabrics containing embedded FR-CD–ICs from direct contact with the FR. Thus, one can envision the use of the most effective FRs with little regard to issues of FR toxicity, if they are delivered in the form of their CD–ICs.

5.2 *Additive-CD–Rotaxanes*

5.2.1 Dyeing with an Azo-Dye-CD–Rotaxane

Soluble additive-CD–rotaxanes can be obtained by first forming a soluble additive-CD–IC, and then attaching bulky groups to both ends of the included guest additive nearest to or extending from the host CD, thereby preventing the unthreading of the additive. Scheme 3 illustrates an example of the synthetic route for obtaining an azo-dye-α-CD–rotaxane [64, 109–111]. The azo-dye-α-CD–rotaxane is water soluble, which is not the case for the original azo-dye. Polyolefin yarns, which are normally pigmented due to their unreactive and hydrophobic surfaces, cannot be dyed without chemical or plasma pretreatments or the introduction of a comonomer. Because it has been demonstrated that CDs have a strong affinity to bind with TiO_2 films [110, 111], when i-PP fibers, containing small amounts of particulate TiO_2 as a delusterant, are heated in aqueous solution of the azo-dye-α-CD–rotaxane, they are quickly dyed.

The characteristics of dyeing i-PP with the azo-dye-α-CD–rotaxane are presented in Fig. 26. Not shown in the figure, however, is that the dyed i-PP yarns are both light and wash fast.

The general procedure of delivering additives in the form of their CD–rotaxanes appears to offer improved solutions to a wide-range of polymer-additive and textile-finishing problems, because of two factors. First, CD–rotaxanation of an additive permits control of its solubility and offers protection (UV and chemical) to the threaded additive. Second, chemical modification of the hydroxyl groups on the

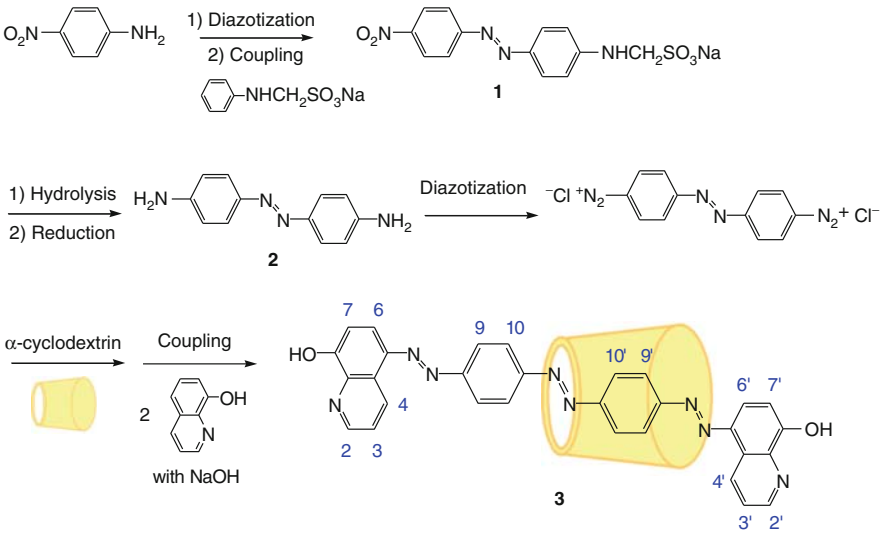

Scheme 3 Synthesis of an azo-dye rotaxane 3 (RD) with 8-hydroxyquinoline as coupling components

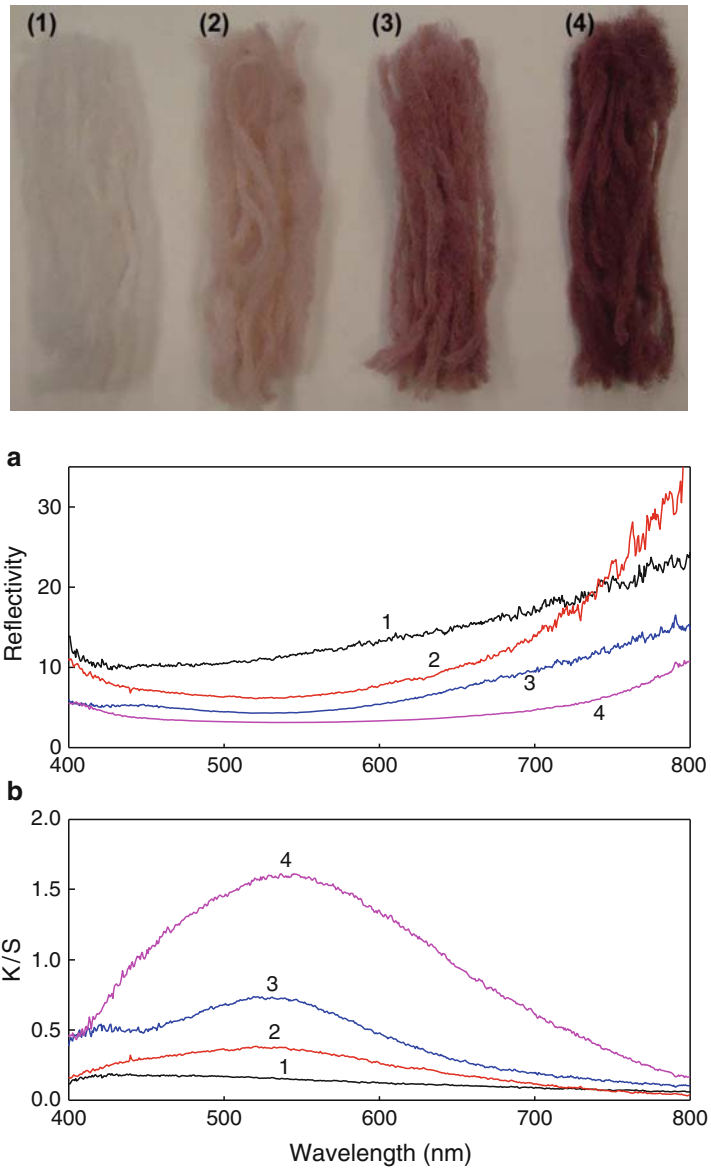

Fig. 26 **1** Reflectivity and **2** K/S curves of PP fibers $K/S = (1–R)^2/2R$, where R = fractional reflectivity, and is a measure of the strength or depth of shade of dyeing. **1** PP before dyeing, **2** after dyed with AzoxFD (free dye), **3** after dyeing with AzoxRD (rotaxanated dye), and **4** after dyeing with AzoxRD complexed with Cu^{2+}. (*Note also photos of the corresponding PP yarns in the top panel*)

CD-coat permits specific substrate targeting of the additive-CD–rotaxane, without the need to modify the chemistry of the additive itself. Together these advantages should soon lead to a new class of polymer and textile additives in the form of their CD–rotaxanes.

5.2.2 Detection of Ni^{+2} with an Azo-Dye-CD–Rotaxane

In fact, recently it has been shown [109] that this same rotaxanated azo-dye is a very sensitive and selective colorimetric and spectrophotometric sensor for nickel(II) salts dissolved in water, showing a submicromolar sensitivity that is highly selective, with a detection range between that of a traditional spectrophotometer and the ion selective electrode (see Figs. 27–29). The effects of anionic species were also studied by adding millimolar amounts of F^-, Cl^-, and HSO_4^{2-} (as their tetrabutylammonium salts) to the Ni^{2+} solution containing the azodye–rotaxane. No interference in the presence of these anionic species for the detection of Ni^{2+} was observed (see Fig. 29).

From elemental analysis, the stoichiometric ratio between Ni^{2+} and the rotaxanated-azo-Dye was 1:1, which shows that the Ni–Dye complex forms linear chains via the hydroxyquinolone ligands. A possible structure of the Ni^{2+}–Dye complex is shown in Scheme 4.

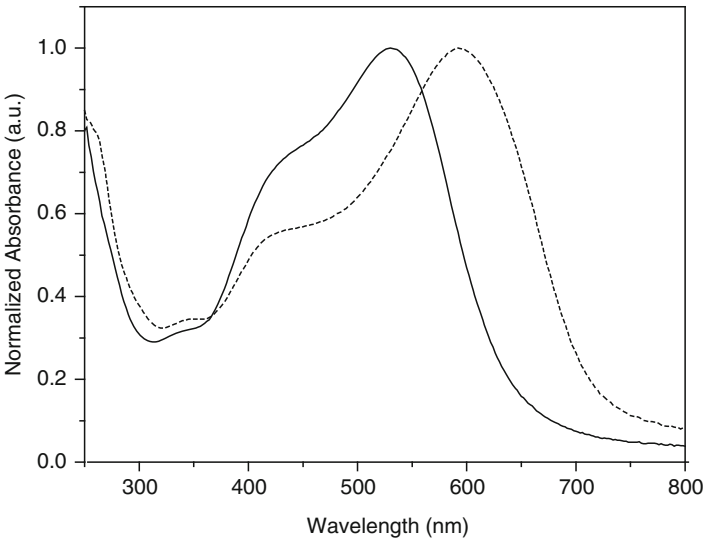

Fig. 27 Normalized UV–Vis absorption spectra in the absence (*solid line*) and presence (*dashed line*) of Ni^{2+} ions added to 3 ml of 20-μM rotaxanated-azo-Dye solution

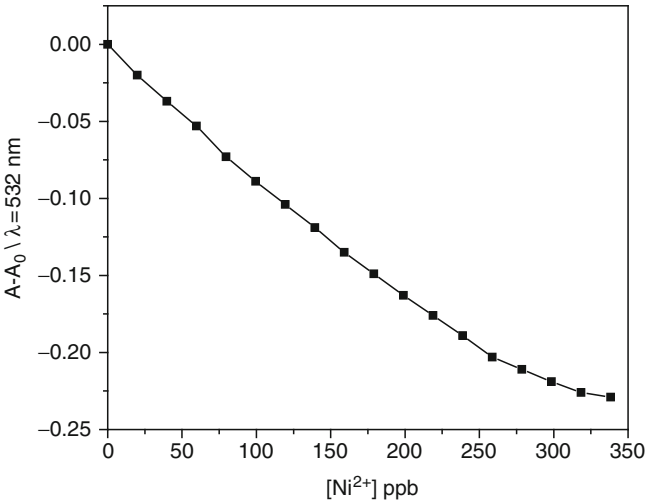

Fig. 28 Titration of the change in the absorption of a rotaxanated-azo-Dye solution measured at ~532 nm vs. the concentration of added Ni^{2+} ions

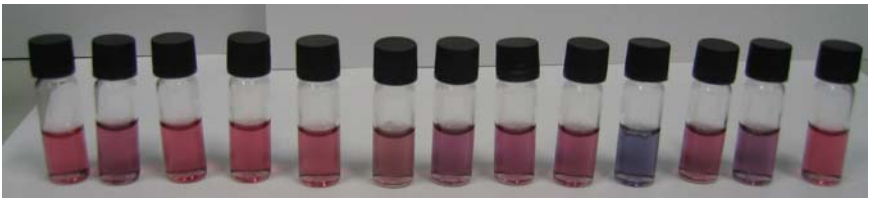

Fig. 29 Color changes observed by "Naked Eye" at very low amounts of M^{+} added (for Ni^{2+} 240 ppb) to 1 ml of the azodye rotaxane solution. From left to right: No metal, $+Hg^{2+}$, $+Ca^{2+}$, $+Mg^{2+}$, $+Fe^{3+}$, $+Fe^{2+}$, $+Cd^{2+}$, $+Cu^{2+}$, $+Co^{2+}$, $+Ni^{2+}$, $+Pb^{2+}$, $+Zn^{2+}$, $+Li^{+}$

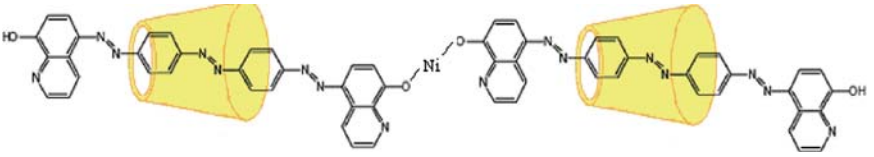

Scheme 4 Possible structure of the 1:1 complex of Ni^{2+} with the rotaxanated-Azo Dye

6 Polymers Functionalized via Covalent Attachment of CDs [112–118]

6.1 Polymers with CDs in their Backbones and as Side Chains

To provide new functionalities to polymer materials, CDs have been chemically bonded to polymers. For example, Sebille et al. [112] grafted β-CD onto

poly-ethyleneimine for the purpose of binding guest drugs. Weickenmeier and Wenz [113] similarly attached β-CDs to the maleic anhydride units in a N-vinyl-2-pyrrolidone/maleic anhydride copolymer, and measured its ability to bind various guest molecules. Here we present several more recent attempts to chemically modify polymers with CDs via covalent bonding.

6.1.1 Step-Growth Polymers

The many hydroxyl groups attached to CDs enable them to be covalently bonded to polymers, either directly to their backbones during, or attached to their side chains subsequent to polymerization. In a modified interfacial polymerization, nylon-6,10 containing various amounts of covalently bonded methyl-β-CDs have been obtained (in methyl-β-CDs two of the three –OHs on each glucose ring are $-OCH_3$) (see Fig. 30) [114–118]. These methyl-β-CD-nylon-6,10 polymers show thermal degradation characteristics very similar to pure nylon-6,10, and are more rapidly dyed to higher dye levels than pure nylon-6,10, as indicated in Fig. 31. Likewise, methyl-β-CD-nylon 6,6 fibers have been synthesized in a similar fashion. DSC data collected for all methyl-β-CD/nylon-6,6 compositions show a characteristic T_m for nylon-6,6 at 255°C, and all are fully soluble in *m*-cresol.

Thus, it is reasonable to assume that the inherent chain mobility of nylon-6,6 is retained in the methyl-β-CD-nylon-6,6s, suggesting that they can be traditionally processed.

6.1.2 Chain-Growth Polymers

Thionyl chloride converts the carboxyl side groups of poly(acrylic acid) to acid chlorides, which will then react with the hydroxyl groups of CD. The degree of CD modification can be varied by controlling the stoichiometry of the CD reaction. Alternatively, the starting material can be a copolymer of acrylic acid or acryloyl chloride with a nonCD-containing comonomer. Incorporation of CD is again achieved by converting the side-groups of the acrylic monomer to CD esters. The CD content of this copolymer can be controlled by varying the initial composition of the copolymer.

Copolymers of acryloyl chloride with methyl methacrylate and styrene have been synthesized, compositional control has been achieved, and the acid chloride side groups have been successfully esterified with methyl-β-CD. One caveat to this method is the difficultly controlling the attachment of just one methyl-β-CD on the reactive side-group, since there are still many hydroxyl groups present on the methyl-β-CD. This then causes methyl-β-CD to act as a crosslinker reacting with several acid chlorides on the copolymer, thereby preventing the methyl-β-CD-incorporated material to be further processed via solution or thermal means.

Mixing low molecular weight PEG with polymers containing CD side groups could lead to a new class of polymer blends in which the polymer A (with CD side

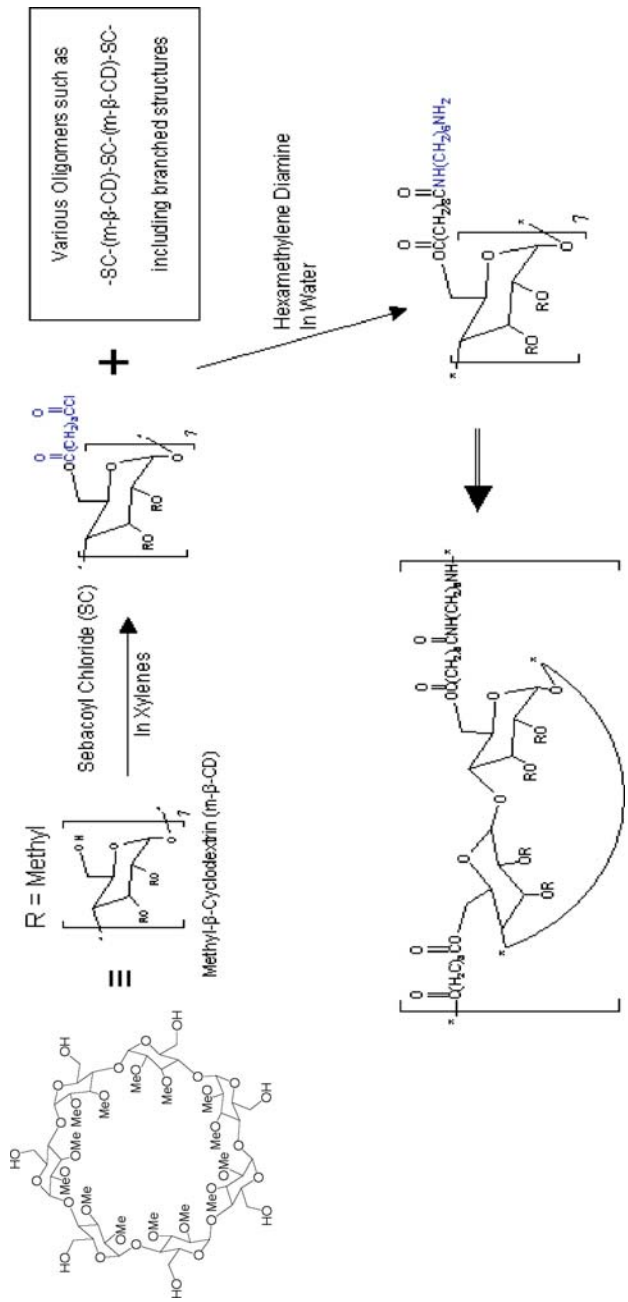

Fig. 30 Synthesis of methyl-β-CD-nylon-6,10 via condensation polymerization using sebacoyl chloride modified methyl-β-CD

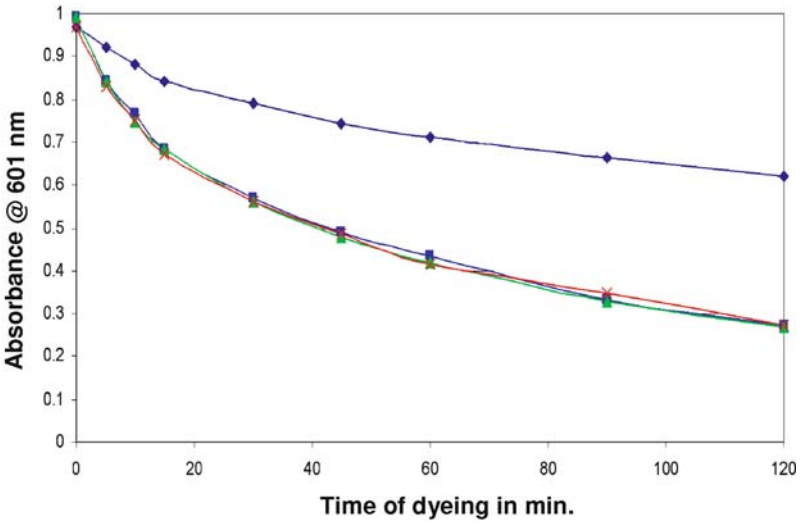

Fig. 31 Disappearance of blue-29 dye from dye bath upon introduction of nylon-6,10 fibers without (*upper curve*) and with (*lower curves*) various contents of covalently bonded methylated-β-CDs in their backbones

groups) is physically crosslinked by polymer B (PEG) through the IC links formed between the CD side groups and PEG. The degree of crosslinking and crosslink length can be controlled simply by varying the amount of PEG added and the PEG chain length, respectively. Using this approach, it may be possible to create a new class of materials which exhibit controllable elastomeric properties.

6.1.3 CD-Star Polymers [114–118]

CDs have several reactive hydroxyl groups, which can be chemically modified and then functionalized with vinyl monomers, such as *t*-butyl acrylate, methyl methacrylate, styrene or acrylonitrile, producing star polymers with CD at their centers (see Fig. 32). One way to control the length of the star arms is through use of atom-transfer radical polymerization (ATRP), which is known to produce highly controlled and uniform polymer molecular weights [119]. This synthetic scheme is applicable to a wide variety of vinyl monomers, and it could become a general method for preparing CD-containing star polymers of differing chemical compositions. Table 8 shows characterization data from our recent work synthesizing stars with a γ-CD core and polystyrene arms [114, 115]. These stars are currently being evaluated for compatibilizing immiscible polymer blends for the purpose of making a more intimately blended system. The theory behind using these CD-stars for compatibilization will be discussed later in this section.

One advantage γ-cyclodextrin has demonstrated is its ability to thread many types of homopolymers into its interior cavity due to its larger inner core dimension of

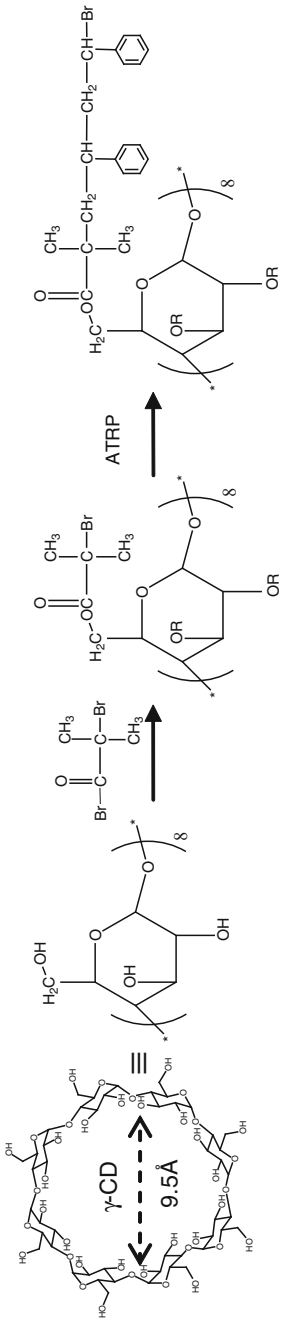

Fig. 32 ATRP synthesis of PS stars with γ-CD core

Table 8 Tabulated characterization results for the PS-γCD-stars [114, 115]

PS_x-gCD[a]	gCD[b] [wt%/mole%]	$Mw_{(actual)}$[b] [g mol^{-1}]	T_g[c] [°C]	Mw[d] [g mol^{-1}]	Mn[d] [g mol^{-1}]	Mw/Mn[d]
PS_0-gCD (initiator)	41.69/7.69	3,085	–	2,060	2047	1.01
$PS_{3.4}$-gCD	17.53/2.39	7,334	87.5	5,465	5,023	1.09
PS_{32}-gCD	2.99/0.26	43,079	96.5	28,826	25,229	1.14
PS_{52}-gCD	1.89/0.16	68,075	99.8	42,317	36,115	1.17
PS_{90}-gCD	1.11/0.09	115,567	109.0	102,035	85,545	1.19

[a] "x" denotes the degree of polymerization per PS arm (average of 12 arms on each γ-CD);
[b] Calculated from ^{1}H-NMR data. MW of modified γ-CD is noted to be *1,286 g mol^{-1}* [$= 1,298\,g\,mol^{-1} - 12$ (H's)] which accounts for the attachment of 12 initiator/arm sites;
[c] Measured with Perkin–Elmer DSC-7 at a heating and cooling rate of 40°/min under air, values represent second heating cycle from 20 to 120°C;
[d] Relative measurements based on SEC linear polystyrene standards in THF

9.5 Å, whereas α- and β-CDs have diameters of 5.7 and 7.8 Å, respectively. A general exception to γ-CD threading has been observed for polystyrene, although this may depend on its tacticity [34, 56]. Isotactic sequences of PS (i-PS) have been modeled [34] to show that threading is possible with a cross-sectional area of 8.9 Å. On the other hand, the cross-sectional diameter of 10.2 Å for syndiotactic PS (s-PS) sequences has been modeled to be too large for threading into the γ-CD cavity [34]. Therefore, an atactic PS (a-PS) containing isotactic sequences on the polymer chain end will have some tendency for inclusion, but full threading of the chain is unlikely. Thus, in theory, using PS for growing arms from the γ-CD core will inherently help to reduce self-threading and thus self-gelation leaving the γ-CD cavity open for other molecular guests.

These star polymers with γ-CD cores have the ability to complex with a variety of additives via formation of CD–ICs. They may also be able to be blended with a second normally incompatible polymer, such as PDMS, with a strong propensity to thread through and complex with their γ-CD cores [14]. Both of these potential applications are illustrated schematically in Fig. 33.

In order to encourage mixing of γ-CD into a given polymer matrix, γ-CD needs to be chemically modified with the same chemical make-up as the matrix polymer to not only make it more compatible with the matrix, but also to break-up and discourage hydrogen bonding between γ-CD hydroxyl groups, which will help to reduce precipitation of crystalline γ-CD and to reduce the heterogeneity of the mixture. Ideally, individual molecules of modified γ-CD will be isolated homogeneously within the matrix (polymer A), where the second homopolymer (polymer B) would be threaded through the γ-CDs, resulting in a homogeneously blended sample. Figure 33 illustrates this concept, where the matrix polymer (polymer A is shown in red, the blended polymer (polymer B) in blue, and the γ-CD in black.

As can be seen, polymer B now has a second possibility for lowering its overall energy, which is accomplished by threading through the cyclodextrin rather than

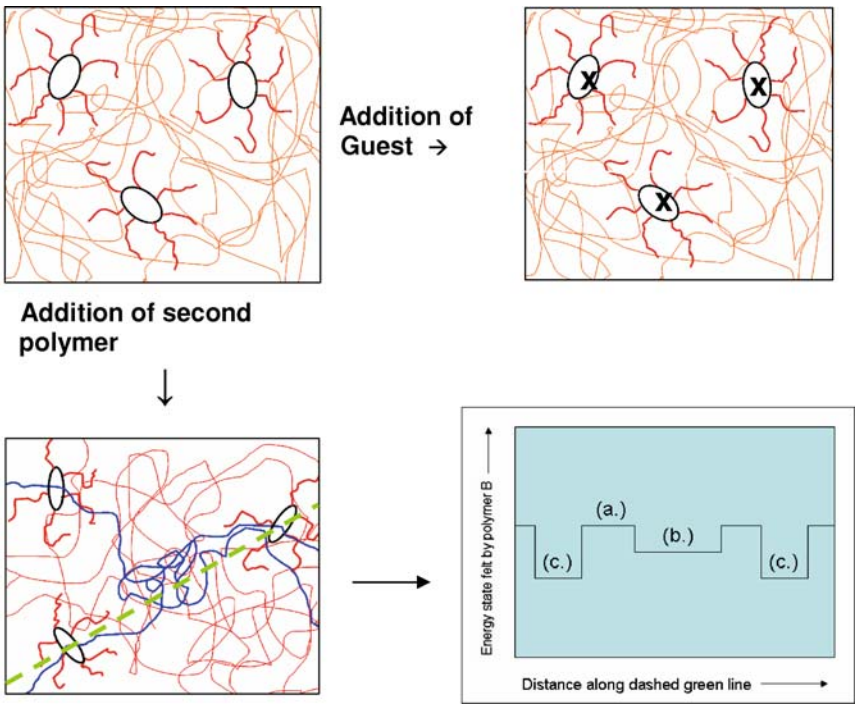

Fig. 33 Complexing small-molecule additive and polymer guests in CD-star polymers. The hypothetical graph in the bottom right corner suggests the relative energy states that may be experienced by polymer B along the *dashed line* in the reference schematic, where (**a**) refers to the A–B energy state, (**b**) to the B–B energy state, and (**c**) is the B–CD energy

coiling into its own phase to maximize B–B interactions. In fact in some polymer cases, if γ-CD is mixed neat into a bulk polymer liquid, an inclusion compound will spontaneously form, indicating that the polymer's environment in the inclusion compound is more energetically favorable than interchain interactions in its bulk [45, 72]. In the lower right corner of Fig. 33, a hypothetical graph of the relative energy states that may be experienced by polymer B along the green dashed line in the schematic shown just to its left in Fig. 33 is suggested. Point (a.) refers to the A–B energy state, (b.) to the B–B energy state, and (c.) is the B–CD energy state.

A point to consider is the physical entrapment of polymer B in the polymer A matrix by the CD "handcuff." If the modified CD is truly dispersed in the matrix polymer, then the polymer-A-modified-CD will be anchored to the polymer A matrix through "like-chain" polymer A–polymer A interactions. So when the blended polymer, polymer B, threads through the CD at that point in the matrix, then the chain motions will be reduced forcing the chain to be channeled through that particular point. This will then lead to kinetic entrapment, which can be viewed as a physical "crosslink," when the temperature is below the glass transition temperature (T_g) of polymer B. For the case when the temperature is above the T_g of polymer

B, it might have enough kinetic energy to wiggle free of the CD handcuff, due to reptilian-like motions, thus becoming able to migrate to another B-chain, where it could possibly lower its overall energy state through B–B interactions, resulting in phase segregation.

Additionally, if both polymers A and B have an affinity for inclusion into cyclodextrin, then the kinetics of IC complexation and competitive lower energy states might need to be carefully considered. To a degree, inclusion may potentially be controlled by molecular weight (MW). Harada et. al. [1] suggested, based on noncompetitive CD–IC formation studies, that there is a much lower probability of CD to find a chain-end for threading higher molecular weight polymers, than for lower MW polymers, thus causing the threading time to be drastically increased [1, 55, 73, 74]. However, in competitive CD–IC formation with polymers of low and high MWs it was found that the CD–ICs formed contained predominantly the high MW polymer. [11, 15, 41]

In Figs. 34 and 35 we present films formed with PS-γ-CD stars and linear PS (MW = 280k) and chloroform solutions containing PS-γ-CD stars, linear PS, and poly(dimethyl siloxane) (PDMS), respectively. The synthesized stars were blended with PS homopolymer to give a 1 wt% γ-CD (7.7 μmols γ-CD core per 1 g) incorporation. The components were initially dissolved in chloroform. After the solvent was removed by evaporation under vacuum and heat, the solid was collected, compression molded under 6 kpsi at 125°C, and quenched to room temperature. The resultant films were clear with a slight yellow tinge. This color is thought to be due to the bromine group capping the end of the PS arms on the stars. These clear and transparent films point to miscibility of the PS-γ-CD-stars in linear PS.

Blending experiments with PS-γ-CD stars were conducted using PDMS, a polymer normally immiscible with PS. The synthesized stars were blended with PS homopolymer (MW = 280 kg mol^{-1}) at a level of 1 wt% γ-CD (7.7 μmols per 1 g)

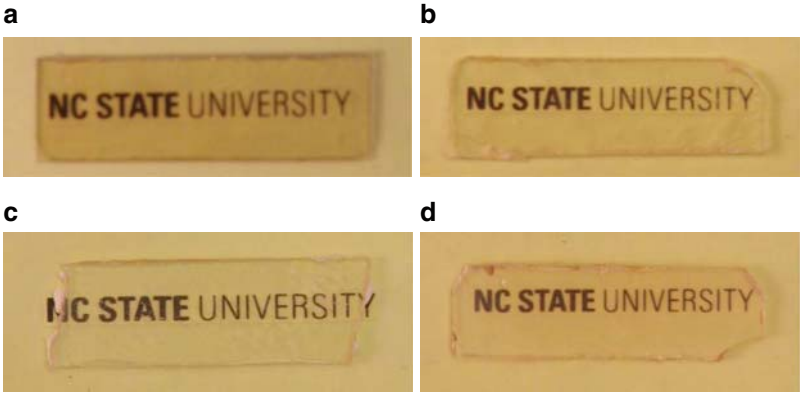

Fig. 34 Images of clear compression molded films made with linear PS (MW = 280 kg mol^{-1}) blended with PS-γ-CD 12-arm star molecules. (**a**) PS3.4-γ-CD, (**b**) PS32-γ-CD, (**c**) PS52-γ-CD, and (**d**) PS90-γ-CD

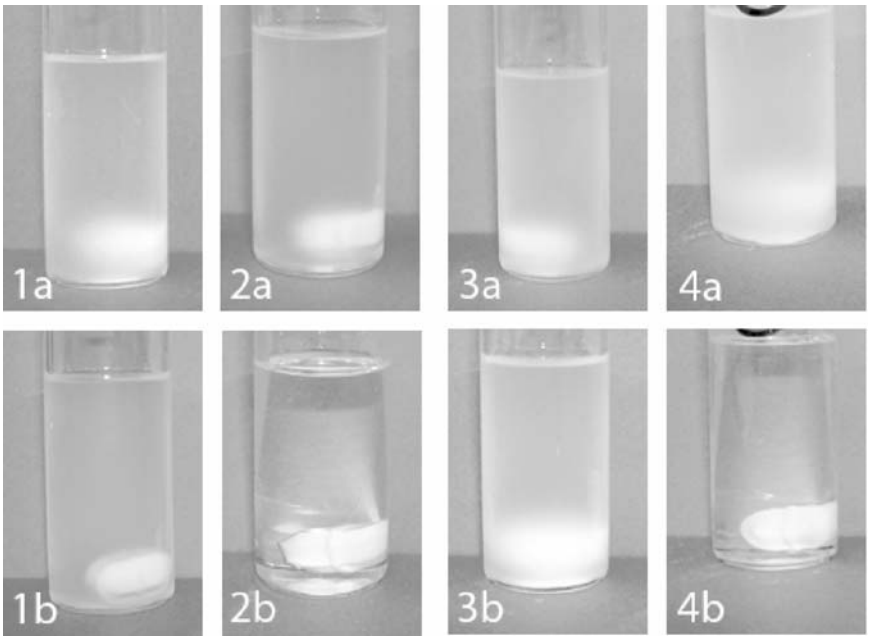

Fig. 35 Before (**a**) and after heating (**b**) solutions to 60°C containing 5 wt% PDMS, where the respective mixtures are made up of (1) PDMS (MW = 62 kg/mol) + PS, (2) PS19γCD star + PDMS (MW = 62 kg mol^{-1}) + PS, (3) PDMS (MW = 308 kg mol^{-1}) + PS, and (4) PS10γCD star + PDMS + PS. Samples containing stars used 1 wt% γ-CD incorporation, where PS (MW = 280 = kg mol^{-1}) made up the remainder of the mass. All solutions had total concentrations of 1 g/10 ml $CHCl_3$. The white masses on the bottom of the vials are PTFE-coated stir bars which can be used to judge the clarity of the solutions

incorporation and 5 wt% PDMS. The degree of polymerization of each star arm (or length) is denoted by the number following the PS designation (e.g., PS90-γ-CD), whereas every star contains 12 arms. Upon mixing the components in chloroform, the solutions were turbid and hazy and remained so after 2 weeks at room temperature. Conversely, heating of these solutions to 60°C for 20–40 h just after preparation resulted in clear solutions. Figure 35 shows images of nonstar and star incorporated solutions before and after heating to 60°C. These solutions were clear and stable for several days after cooling back to room temperature. The stirbar at the bottom of the vials can be used to gauge the clarity of the solutions. Clearing of the solutions containing the stars, illustrated in Fig. 35, provides evidence pointing to threading of PDMS though the γ-CD cores.

Figure 36 shows differential scanning calorimetry heating traces comparing films processed identically from select solutions in Fig. 35. It can be observed that the sample containing only PDMS + PS shows evidence of a T_m at −39°C due to the PDMS, whereas the sample containing star + PDMS + PS does not show a T_m in this region due to the PDMS. This leads to the notion that the PDMS is molecularly dispersed and not able to crystallize, which is a result of the PDMS being

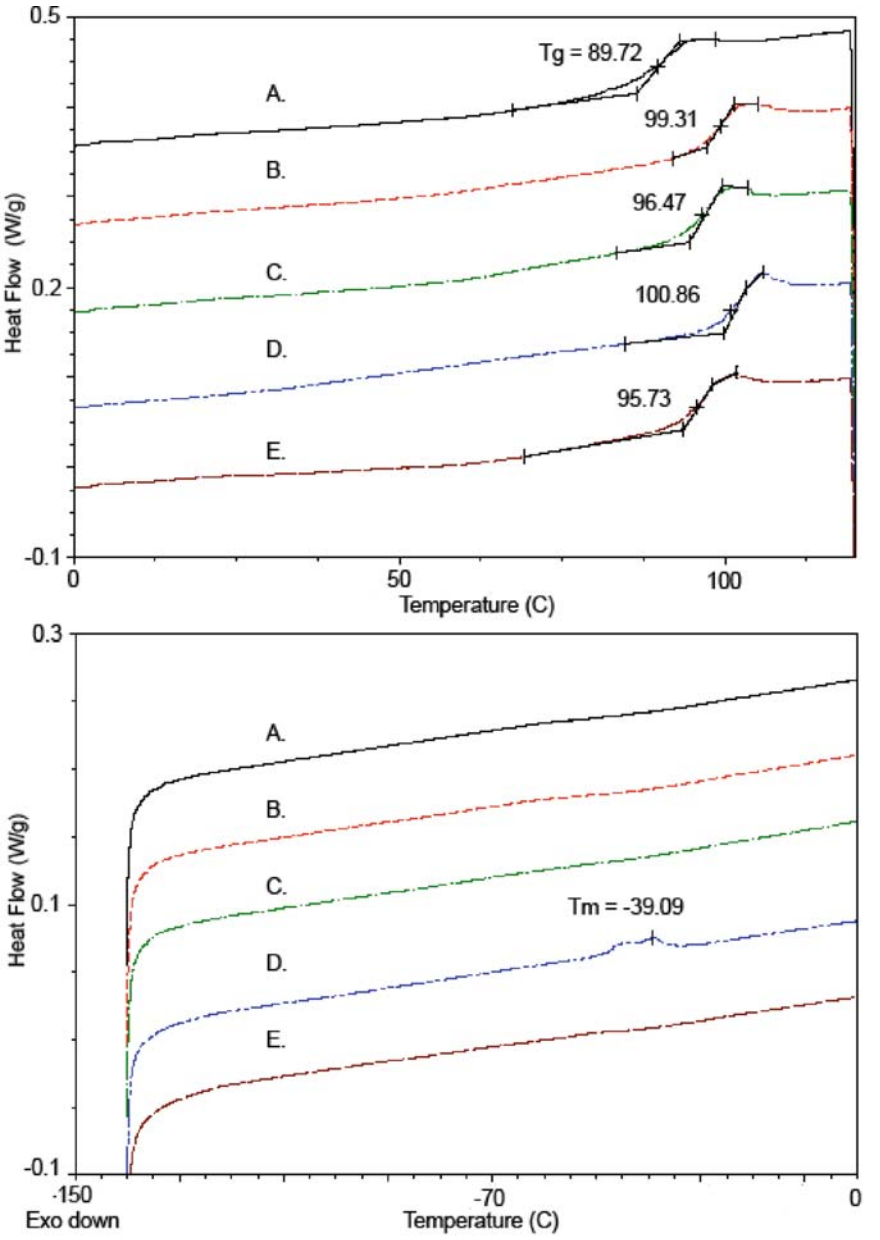

Fig. 36 Differential Scanning Calorimeter traces of (**a**) PS10-γ-CD star, (**b**) PS, (**c**) PS10-γ-CD star + PS, (**d**) PDMS + PS, and (**e**) PS10-γ-CD star + PDMS + PS. The star containing sample incorporated 1 wt% γ-CD, whereas samples containing PDMS (MW = 308 kg mol^{-1}) incorporated 5 wt%, while with the remainder of the mass was composed of PS (MW = 280 kg mol^{-1}). All DSC curves present the second heating cycle for each sample at a heating rate of 10°C min^{-1} under helium purge gas

physically handcuffed into the PS matrix by the cyclodextrin star leading to reduced molecular interactions and motions. Further evidence of molecular mixing is the PS glass transition (T_g) region for the star + PDMS + PS sample. In this region the T_g of the star + PDMS + PS sample is slightly reduced to 95.7°C when compared to only star + PS, which has a T_g of 96.5°C. Overall the DSC data suggests that at least partial intimate blending is occurring.

7 Summary and Conclusions

We have demonstrated that the structures, morphologies, and even chain conformations of solid polymer samples may be altered by including them in and then coalescing them from their CD–ICs. In addition to altering their physical behaviors, coalescence of guest polymers from their CD–ICs permits us to obtain solid polymer samples that are distinct from bulk samples made from their solutions and melts. Clearly study of such reorganized coalesced polymer samples can contribute to our ability to understand and develop improved structure–property relations for them.

Additionally, because crystalline CD–ICs are high-melting and thermally stable, even when containing small-molecule guests that are volatile liquids or even gases in the bulk, delivery of additives to polymer materials can be improved by using additive-CD–ICs, which may often be conveniently melt-processed into polymers. If we begin with appropriate soluble additive-CD–IC and then react the unincluded ends of the guest additive with capping groups that prevent it from unthreading, we create a CD-additive-rotaxane. One advantage of CD-additive-rotaxanes is the protection (thermal, chemical, UV–Vis, etc.) afforded by their CD coats. Another is the ability to utilize the many –OH groups on the CD coat to target the delivery of the CD-additive-rotaxane to a particular polymer substrate.

CDs may also be covalently bonded to polymers to alter their functionalities through incorporation of CDs into their backbones during polymerization or attachment to their side-chains via postpolymerization reactions. The presence of covalently bonded CDs in polymers serves to increase their acceptance and retention of additives, such as dyes, fragrances, antibacterials, etc. They may also be further reacted or treated through their covalently bonded CDs to cross-link and form networks or to form blends with other polymers having a propensity to thread through their attached CD cavities.

Because CDs are nontoxic, biodegradable, and bioabsorbable, they may be used in medical applications, as well as providing for the fabrication of more environmentally responsible polymer materials. In this report we have summarized almost exclusively our own recent studies employing the cyclic starch derivatives called cyclodextrins to both nanostructure and functionalize polymer materials. Lest the reader gets the erroneous impression that our studies have been carried out in isolation, we refer to a recent review [120], and a summary [121], describing related

research that also attempts to utilize CDs and polymers to create materials with improved and new properties for advanced applications.

Acknowledgements I am grateful to the many students and collaborators listed in the references that have made possible the research described herein. Funding received from the National Textile Center (U.S. Commerce Dept.), the National Science Foundation, and North Carolina State University is appreciated. I am also grateful to the editor of this Volume, Prof. Gerhard Wenz, for his careful reading of this chapter and for his useful suggestions.

References

1. Harada A, Kamachi M (1990) Macromolecules 23:2821
2. Huang L, Vasanthan N, Tonelli AE (1997) J Appl Polym Sci 64:281
3. Tonelli AE (1997) Polym Int 43:295
4. Huang L, Allen EJ, Tonelli AE (1997) In: Pandalai SG (ed) Recent research developments in macromolecular research, Vol. 2. Research Signpost, Trivandrum, India, p 175
5. Huang L, Allen E, Tonelli AE (1998) Polymer 39:4857
6. Huang L, Tonelli AE (1998) J Macromol Sci Revs Macromol Chem Phys C38(4):781
7. Huang L, Tonelli AE (1999) In: Dinh SM, DeNuzzio JD, Comfort AR (eds) Intelligent materials for controlled release technologies, Chap.10. ACS Symposium Series No. 728. ACS, Washington, DC
8. Huang L, Allen E, Tonelli AE (1999) Polymer 40:3211
9. Huang L, Taylor H, Gerber M, Orndorff P, Horton J, Tonelli AE (1999) J Appl Polym Sci 74:937
10. Lu J, Shin ID, Nojima S, Tonelli AE (2000) Polymer 41:5871
11. Rusa CC, Tonelli AE (2000) Macromolecules 33:1813
12. Rusa CC, Tonelli AE (2000) Macromolecules 33:5321
13. Huang L, Gerber M, Lu J, Tonelli AE (2001) Polym Degrad Stabil 71:279
14. Porbeni FE, Edeki EM, Shin ID, Tonelli AE (2001) Polymer 42(16):6907
15. Rusa CC, Luca C, Tonelli AE (2001) Macromolecules 34:1318
16. Wei M, Tonelli AE (2001) Macromolecules 34:4061
17. Lu J, Hill M, Hood M, Greeson DF Jr, Horton IR, Orndorff PE, Herndon SA, Tonelli AE (2001) J Appl Polym Sci 82:300
18. Shuai X, Porbeni FE, Wei M, Shin ID, Tonelli AE (2001) Macromolecules 34:7355
19. Huang L, Gerber M, Taylor H, Lu J, Tapazsi E, Wutkowski M, Hill M, Harvey A, Rusa CC, Wei M, Porbeni FE, Lewis CS, Tonelli AE (2001) Macromol Chem Macromol Sympos 176:129
20. Shuai X, Wei M, Porbeni FE, Bullions TA, Tonelli AE (2002) Biomacromolecules 3:201
21. Bullions TA, Wei M, Porbeni FE, Gerber MJ, Peet J, Balik M, Tonelli AE (2002) J Polym Sci Polym Phys Ed 40:992
22. Shuai X, Porbeni FE, Wei M, Bullions TA, Tonelli AE (2002) Macromolecules 35:3126
23. Wei M, Davis W, Urban B, Song Y, Porbeni FE, Wang X, White JL, Balik CM, Rusa CC, Fox J, Tonelli AE (2002) Macromolecules 35:8039
24. Rusa CC, Bullions TA, Fox J, Porbeni FE, Wang X, Tonelli AE (2002) Langmuir 18:10016
25. Shuai X, Porbeni FE, Wei M, Bullions TA, Tonelli AE (2002) Macromolecules 35:2401
26. Shuai X, Porbeni FE, Wei M, Bullions TA, Tonelli AE (2002) Macromolecules 35:3778
27. Wei M, Shuai X, Tonelli AE (2003) Biomacromolecules 4:783
28. Bullions TA, Edeki EM, Porbeni FE, Wei M, Shuai X, Tonelli AE (2003) J Polym Sci Polym Phys Ed 41:139
29. Rusa CC, Fox J, Tonelli AE (2003) Macromolecules 36:2742

30. Abdala AA, Khan S, Tonelli AE (2003) Macromolecules 36:7833
31. Tonelli AE (2003) J Tex. Appar Tech Manage 3(2):1
32. Tonelli AE (2003) Macromol Sympos 203:71
33. Wei M, Bullions TA, Rusa CC, Wang X, Tonelli AE (2003) J Polym Sci B Polym Phys Ed 42:386

As seen in Fig. 10 in both non-aromatic carbon spectral regions the least shielded, downfield resonance belongs to as-received PET, the most shielded, upfield resonance comes from coalesced or included PETs, and the precipitated PET [59] seems to contain ∼30 and ∼70% material resonating at the frequencies of these downfield and upfield, as-received, and coalesced or included PET peaks, respectively. We expect [122] carbonyl carbons terminating ethylene glycol fragments whose -CH_2–O- and -O–CH_2- bonds have g± conformations to resonate upfield from those with t conformations. This is consistent with conclusions drawn previously from modeling the conformations of included PET chains [78, 84] and the FTIR analysis [21] of as-received and coalesced PET conformations.

We would normally expect the methylene carbon resonances of these PET samples to exhibit the same order of resonance frequencies, because they are γ to the carbonyl carbons and are either t or g± to them conformationally across the same -CH_2–O- and -O–CH_2- bonds. This is, in fact, what we observe in Fig. 10. However, a recent solid-state ^{13}C-NMR study of PETs by Kaji and Schmidt-Rohr [123] has convincingly established that the resonance frequencies of methylene carbons in PETs are insensitive to the conformations of the -CH_2–O- and -O–CH_2- bonds, and instead seem to depend only upon the conformations of the -CH_2–CH_2- bond connecting them. On highly crystalline and predominantly amorphous PET samples with ^{13}C-enriched methylene carbons they were able to separately observe methylene carbon resonances belonging to t and to g ± -CH_2–CH_2- bonds. They found that in both PET samples the methylene carbons belonging to t -CH_2–CH_2- bonds resonated ∼2 ppm upfield from those methylene carbons with g ± -CH_2–CH_2- bonds, even though the -CH_2–O- and -O–CH_2- bonds are predominantly t in the highly crystalline PET and significantly g± in the nearly completely amorphous PET sample. As a consequence, we can conclude that our coalesced and included PETs have predominantly t -CH_2–CH_2- bonds, as-received PET predominantly g±, and our precipitated PET [59] sample seems to have about 30% g± and 70% t -CH_2–CH_2 bonds. Again, this is consistent with our molecular modeling [78, 84] and FTIR [21] results, so as-received PET has predominantly g ± -CH_2–CH_2- bonds and substantial amounts of t -CH_2–O- and -O–CH_2- bonds, while coalesced, included, and precipitated PETs have preponderantly t -CH_2–CH_2- and g ± -CH_2–O- and -O–CH_2- bonds.

The ^{13}C-observed ^{1}H spin-lattice relaxation times observed in the rotating frame [$T_{1\rho}(^1H)$], which reflect motions in the kHz frequency regime, are presented as a function of temperature for our PET samples in Fig. 11. Generally the coalesced sample has the longest and the as-received sample the shortest $T_{1\rho}(^1H)$, indicating an increasing kHz mobility for PET chains in the coalesced, precipitated, and as-received samples, respectively. Also note that the $T_{1\rho}(^1H)$s of as-received PET show a marked sensitivity to temperature at $T \sim T_g$, which is largely unobserved in the coalesced and precipitated samples. Initially, the molecular motion increases with temperature resulting in shorter $T_{1\rho}(^1H)$s for all the PET samples. However, the $T_{1\rho}(^1H)$ of the as-received PET reaches a minimum near T_g, and further heating results in molecular motions that are too rapid for efficient nuclear spin energy transfer, so $T_{1\rho}(^1H)$ increases for $T > T_g$. This is consistent with the presence and absence of a glass transition observed in the DSC scans of as-received and coalesced (see Fig. 7) or precipitated [59] PETs, respectively. Thus, both macroscopic (DSC) and microscopic (NMR) observations point to the absence of a glass transition in the noncrystalline regions of coalesced or precipitated PETs.

At room temperature, the ^{13}C spin-lattice relaxation times, $T_1(^{13}C)$ in seconds, for the as-received (asr), precipitated (ppt), and coalesced (coa) PETS are $C = O \rightarrow 31.8\,s$ (asr) and 36.2 s (coa, ppt); nonprotonated aromatic $\rightarrow 28.6\,s$ (asr) and 36.2 (coa, ppt); protonated aromatic $\rightarrow 14.4\,s$ (asr) and 21.0 s (coa, ppt); and $CH_2 \rightarrow 7.1\,s$ (asr) and 9.6 s (coa, ppt).

Coalesced and precipitated PETs have longer $T_1(^{13}C)$s than as received PET. Thus, motions in the MHz frequency regime are also more restricted in the coalesced and

precipitated PETs, compared with as-received PET, possibly because of both their higher crystallinities and the tighter packing of kink conformers in their noncrystalline regions. Temperature dependencies similar to those observed in the rotating frame for ^1Hs, $T_{1\rho}(^1H)s$, are also observed for the $T_1(^{13}C)s$. This behavior implies that the noncrystalline regions of coalesced and precipitated PETs are distinct from the amorphous regions in as-received PET, because only in as-received PET are the kHz, MHz motions important to $T_{1\rho}(^1H)$ and $T_1(^{13}C)$ relaxations sensitive to whether or not the sample is below or above its T_g. This is again consistent with the failure to observe a glass transition by DSC for coalesced [21] and precipitated [33, 59] PETs.

34. Hunt MA, Uyar T, Shamsheer R, Tonelli AE (2004) Polymer 45:1345
35. Rusa CC, Uyar T, Rusa M, Hunt MA, Wang X, Tonelli AE (2004) J Polym Sci B Polym Phys Ed 42:4182
36. Abdala AA, Wu W, Olesen K, Jenkins RD, Tonelli AE, Khan S (2004) J Rheol 48:979
37. Wei M, Shin ID, Urban B, Tonelli AE (2004) J Polym Sci B Polym Phys Ed 42:1369
38. Rusa CC, Shuai X, Bullions TA, Wei M, Porbeni FE, J. Lu, L. Huang, J. Fox, Tonelli AE (2004) J Polym Environ 12(3):157
39. Rusa CC, Wei M, Bullions TA, Rusa M, Gomez MA, Porbeni FE, Wang X, Shin ID, Balik CM, White JL, Tonelli AE (2004) Cryst Growth Design 4:1431
40. Rusa CC, Wei M, Shuai X, Bullions TA, Wang X, Rusa M, Uyar T, Tonelli AE (2004) J Polym Sci B Polym Phys Ed 42:4207
41. Rusa M, Wang X, Tonelli AE (2004) Macromolecules 37:6898
42. Rusa CC, Rusa M, Gomez MA, Shin ID, Fox JD, Tonelli AE (2004) Macromolecules 37:7992
43. Hernandez R, Rusa M, Rusa CC, Lopez D, Mijanos C, Tonelli AE (2004) Macromolecules 37:9620
44. Rusa CC, Wei M, Bullions TA, Shuai X, Uyar T, Tonelli AE (2005) Polym Adv Technol 16:269
45. Peet J, Rusa CC, Hunt MA, Tonelli AE, Balik CM (2005) Macromolecules 38:537
46. Jia X, Wang X, Tonelli AE,White JL (2005) Macromolecules 38:2775
47. Uyar T, Rusa CC, Wang X,Rusa M, Hacaloglu J, Tonelli AE (2005) J Polym Sci B Polym Phys Ed 43:2578
48. Rusa CC, Bridges C,Ha S-W, Tonelli AE (2005) Macromolecules 38:5640
49. Uyar T, Rusa CC, Hunt MA, Aslan E, Hacaloglu J, Tonelli AE (2005) Polymer 46:4762
50. Porbeni FE, Shin ID, Shuai X, Wang X, White JL, Jia X, Tonelli AE (2005) J Polym Sci B Polym Phys 43:2086
51. Uyar T, Aslan E, Tonelli AE, Hacaloglu J (2006) Polym Degrad Stabil 91(1):1
52. Uyar T, El-Shafei A, Hacaloglu J, Tonelli AE (2006) J Inclus Phenom Macrocyc Chem 55:109
53. Uyar T, Hunt MA, Gracz HS, Tonelli AE (2006) Cryst Growth Design 6:1113
54. Uyar T, Oguz G, Tonelli AE, Hacaloglu J (2006) Polym Degrad Stabil 91:2471
55. Rusa CC, Rusa M, Peet J, Uyar T, Fox J, Hunt MA, Wang X, Balik CM, Tonelli AE (2006) J Inclus Phenom Macrocyc Chem 55:185
56. Uyar T, Gracz HS, Rusa M, Shin ID, El-Shafei A, Tonelli AE (2006) Polymer 47:6948
57. Uyar T, Tonelli AE, J. Hacaloglu (2006) Polym Degrad Stabil 91:2960
58. Pang K, Schmidt B, Kotek R, Tonelli AE (2006) J Appl Polym Sci 102(6):6049
59. Vedula J, Tonelli AE (2007) J Polym Sci B Polym Phys Ed 45:735 (Here the slow addition of a heated trifluoroacetic acid solution of PET into rapidly stirred acetone resulted in a precipitated PET sample (p-PET) whose physical behaviors closely parallel those of PET coalesced from its γ-CD-IC.)
60. Tonelli AE (2007) In: Brown P, Stevens K (eds) Handbook of nanofiber & nanotechnology in textiles. Woodhead, Cambridge, UK
61. Paik Y, Poliks B, Rusa CC, Tonelli AE, Schaefer J (2007) J Polym Sci Part B Polym Phys Ed 45:1271
62. Uyar T, Rusa CC, Tonelli AE, Hacaloglu J (2007) Polym Degrad Stabil 92:32
63. Martinez G, Gomez MA, Villar S, Garrido L, Tonelli AE, Balik CM (2007) J Polym Sci A Polym Chem 45:2503
64. Park JS, Tonelli AE, Srinivasaro M (2009) Adv Mater YY:xxxx

65. Whang H-S, Medlin E, Wrench N, Hockney J, Farin CE, Tonelli AE (2007) J Appl Polym Sci 106:4104
66. Yang H, El-Shafei A, Schilling FC, Tonelli AE (2007) Macromol Theor Simul 16:797
67. Tonelli AE (2008) J Inclus Phenom Macrocyc Chem 60:197
68. Whang H-S, Vendeix FAP, Gracz HS, Gadsby J, Tonelli AE (2008) Pharm Res 25:1142
69. Whang H-S, Hunt MA, Medlin E, Wrench N, Hockney J, Farin CE, Tonelli AE (2007) J Appl Polym Sci 106:4104
70. Whang H-S, Tonelli AE (2008) J Inclus Phenom Macrocyc Chem 62:127
71. Steinbrunn MB, Wenz G (1997) DE 19707855.9, PCT/DE 98/0056
72. Harada A, Okada M, Kawaguchi Y (2007) Chem Lett 34:542
73. Wenz G, Han BH, Muller A (2006) Chem Revs 106(3):782
74. Harada A, Hashidzume A, Takashima Y (2006) Adv Polym Sci 201:1
75. Wenz G (2008) Molecular Recognition of Polymers by Cyclodextrins. Adv Polym Sci
76. Tonelli AE (1991) Theor Comput Polym Sci 1:22
77. Hunt MA, Tonelli AE, Balik CM (2007) J Phys Chem 111:3853
78. Tonelli AE (1992) Comp Theor Polym Sci 2:80
79. Koenig JL (1992) Spectroscopy of polymers, Chap. 4. American Chemical Society, Washington, DC
80. Zerbi G (1999) Modern polymer spectroscopy, Chap. 3. Wiley, New York
81. Miyake A (1959) J Polym Sci 38:479
82. D'Esposito L, Koenig JL (1976) J Polym Sci Polym B Polym Phys Ed 14:1731
83. Psarski M, Piorkowska E, Galeski A (2000) Macromolecules 33:916
84. Tonelli AE (2002) Polymer 43:637
85. Natta G, Corradini P (1960) Nuovo Cim Suppl 15:40
86. Turner-Jones A, Aizlewood JM, Beckett DR (1964) Makromol Chem 75:134
87. Gomez MA, Tanaka H, Tonelli AE (1987) Polymer 28:2227
88. Tonelli AE (1991) Macromolecules 24:3069
89. Eaton P, Vasanthan N, Tonelli AE (1995) Macromolecules 28:2531
90. Belfiore LA, Schilling FC, Tonelli AE, Lovinger AJ, Bovey FA (1984) Macromolecules 17:2561
91. Nakamura K, Aioke K, Usaka K, Kanamoto T (1999) Macromolecules 32:4975
92. Wenz G, Steinbrunn MB (1997) (University of Karlsruhe (TH), Germany). De 19608354 Chem Abstr:623641
93. Steinbrunn MB, Wenz G (1996) Angew Chem Int Ed 35:2139
94. Wenz G, Steinbrunn MB, Landfester K (1997) Tetrahedron 53:15575 (for inclusion and coalescence of nylon-11 from α-CD)
95. Vashanthan N, Salem D (2001) J Polym Sci Polym B Phys Ed 39:536
96. Willcox PJ, Howie DW, Schmidt-Rohr K, Hoagland DA, Gido SP (1999) J Polym Sci Pol Phys 37:3438
97. Hassan CM, Peppas NA (2000) Adv Polym Sci 153:37
98. Hernández R, López D, Mijangos C, Guenet JM (2002) Polymer 43:5661
99. Hernandez R, Sarafian A, López D, Mijangos C (2004) Polymer 45:5543
100. http://www.gl.iit.edu/frame/genbank.htm, Fibroin heavy chain precursor (Fib-H) (H- fibroin), gij9087216jspjP05790j FBOH_BOMMO[9087216], Gene Bank
101. Li J, Ni X, Zhou Z, Leong KW (2003) J Am Chem Soc 125:1788
102. Girardeau TE, Zhao T, Leisen J, Beckham HW (2005) Macromolecules 38:2261
103. He Y, Inoue Y (2003) Biomacromolecules 4:1865
104. Vogel R, Tandler B, Haussler L, Jehnichen D, Brunig H (2006) Macromol Biosci 6:730
105. Dong T, He Y, Zhu B, Shin K, Inoue Y (2005) Macromolecules 38:7736
106. Dong T, Shin K, Zhu B, Inoue Y (2006) Macromolecules 39:2427
107. Kawaguchi Y, Nishiyama T, Okada M, Kamachi M, Harada A (2000) Macromolecules 33:4427
108. Lu J, Mirau PA, Tonelli AE (2001) Macromolecules 34:3276
109. Park JSK, Srinivasaro M (2009) Macromolecules YY:xxxx
110. Haque SA, Park JS, Srinivasarao M, Durrant JR (2004) Adv Mater 16(14):1177

111. Craig MR, Claridge TDW, Hutchings MG, Anderson HL (1999) Chem Commun 1537
112. Sebille B, Thuaud N, Behar N, Piquion J (1987) J Chromatogr 409:61
113. Weickenmeier M, Wenz G (1996) Macromol Rapid Commun 17:731
114. Busche BJ, Balik CM (2006) Abstr Pap Am Chem Soc 231:2
115. Busche BJ, Tonelli AE, Balik CM (2007) Abstr Pap Am Chem Soc 232:2
116. Miura Y, Narumi A, Matsuya S, Satoh T, Duan Q, Kaga H, Kakuchi T (2005) J Polym Sci A Polym Chem 43:4271
117. Xiao H, Li J (2005) Tetrahedron Lett 46:2227
118. Plamper FA, Becker H, Lanzendorfer M, Patel M, Wittemann A, Ballauf M, Muller AHE (2005) Macromol Chem Phys 206:1813
119. Odian G (2004) Principles of polymerization, Chap. 3, 4th edn. Wiley, New York
120. Wenz G, Han BH, Muller A (2006) Chem Rev 106(3):782
121. Volume 57 of J. Inclusion Phenom Macrocyclic Chem 2007, is devoted to papers presented at the XIII International Cyclodextrin Symposium held May, 2006 in Turin, Italy.
122. Tonelli AE (1989) NMR spectroscopy and polymer microstructure: the conformational connection. VCH, New York
123. Kaji H, Schmidt-Rohr K (2002) Macromolecules 35:7993